A HARMONIC FUNCTION METHOD FOR EEG SOURCE RECONSTRUCTION

by

HONGGUANG XI

Presented to the Faculty of the Graduate School of

The University of Texas at Arlington in Partial Fulfillment

of the Requirements

for the Degree of

DOCTOR OF PHILOSOPHY

THE UNIVERSITY OF TEXAS AT ARLINGTON

December 2016

To my mother Lingying and my late father Dilong

to whom I owe too much.

ACKNOWLEDGEMENTS

I would like to thank my supervising professor Dr. Jianzhong Su for constantly motivating and encouraging me, and also for his invaluable advice during the course of my doctoral studies. I wish to thank Dr. Guojun Liao, Dr. Andrzej Korzeniowski, and Dr. Hristo Kojouharov for their interest in my research and for taking time to serve in my dissertation committee.

I wish to thank Dr. Hanli Liu, Dr. Yuanbo Peng, Dr. Shouyi Wang, Olajide Babawale, and Haley Harris, for providing the experiment data and giving me helpful guidance in research. I am especially grateful to Dr. Marc Turcotte for his support and help in my most difficult time. I wish also to thank Dr. Georgios Alexandrakis and Dr. Quan-Zhen Li for offering me opportunities to enhance my skills in science and engineering.

My colleagues, Dr. Pengcheng Xiao, Sat Byul Seo, Ariel Bowman, Dr. Yueming Liu, Dr. Honghui Zhang, Gaoxiang Yang, Dr. Denggui Fan, Dongpo Hu, Dr. Zigen Song, Dr. Ying Du, and Suyu Liu, give me a lot of help, corrections and suggestions. I hope to deliver a hearty thank you to them all.

Finally, I would like to express my profound appreciation to my family for their love, support, and tolerance.

November 15, 2016

ABSTRACT

A HARMONIC FUNCTION METHOD FOR EEG SOURCE RECONSTRUCTION

HONGGUANG XI, Ph.D.

The University of Texas at Arlington, 2016

Supervising Professor: Jianzhong Su

Neuronal activities generate the electrical current in the brain, and further result in the potential changes over the scalp. Electroencephalography (EEG) is a technique used to record the potential changes on the scalp.

Even though fMRI, PET, MEG and other brain-imaging tools are widely used in brain research, they are limited by low spatial/temporal resolution, cost, mobility and suitability for long-term monitoring. In contrast, EEG signals have been successfully used to obtain useful diagnostic information (neural oscillations and response times) in clinical contexts. Further, they present the advantage to be highly portable, inexpensive, and can be acquired at the bedside or in real-life environments with a high temporal resolution.

In this dissertation we study a harmonic function method for dipolar source reconstruction, and apply the method to the real pain data. We first propose a new

error estimate that is different from an earlier result of Chafik *et al.* and we provide a rigorous proof of the estimate. We then validate our method in computer-simulated data and study its numerical stability in different noise levels. Finally, we apply the method to EEG data acquired in pain experiments. Our result shows that when the hand is in the cold water there are strong activities near the prefrontal cortex and the anterior cingulate cortex, which is consistent with the known knowledge in neuroscience.

Though the harmonic function method is affected by the noise level, its simplicity and beauty make it a promising method for further development in EEG source reconstruction.

TABLE OF CONTENTS

LIST OF ILLUSTRATIONS

Figure | Page

LIST OF TABLES

CHAPTER 1

Introduction

Neuronal activities generate the electrical current in the brain, and further result in the potential changes over the scalp. Electroencephalography (EEG) is a technique used to record the potential changes on the scalp.

Even though fMRI, PET, MEG and other brain-imaging tools are widely used in brain research, they are limited by low spatial/temporal resolution, cost, mobility and suitability for long-term monitoring. For example, fMRI has the advantage of providing spatially-resolved data, but suffers from an ill-posed temporal inverse problem, i.e., a map with regional activations does not contain information about when and in which order these activations have occurred [1]. In contrast, EEG signals have been successfully used to obtain useful diagnostic information (neural oscillations and response times) in clinical contexts. Further, they present the advantage to be highly portable, inexpensive, and can be acquired at the bedside or in real-life environments with a high temporal resolution. Because of the lack of significant patient risks, EEG is additionally suited for long-term monitoring.

EEG offers the possibility of measuring the electrical activity of neuronal cell assemblies on the sub-millisecond time scale [2, 3, 4]. EEG source imaging further identifies the positions or distributions of electric fields based on EEG signals collected on the scalp [5]. This new tool is widely used in cognitive neuroscience research, and has also found important applications in clinical neuroscience such as neurology, psychiatry and psychopharmacology. In cognitive neuroscience, the majority of the studies investigate the temporal aspects of information processing by analyzing event related potentials (ERP). In neurology, the study of sensory or motor evoked potentials is of increasing interest, but the main clinical application concerns with the localization of epileptic foci. In psychiatry and psychopharmacology, a major focus of interest is the localization of sources of certain EEG frequency bands. Localizing the activity sources of a given scalp EEG measurement is achieved by solving the so-called inverse problem [6]. These kinds of inverse problems are usually ill-posed and their solutions are non-unique [7, 8].

El Badia and Ha-Duong [9] established an algebraic method to identify the number, locations and moments of electrostatic dipoles in 2D or 3D domain from the Cauchy data on the boundary. Chafik *et al.* [10] further provided an error estimate without proof.

Nara and Ando [11] provided a new projective method for 3D source reconstruction by projecting the sources onto a Riemann sphere.

Kang and Lee [12] proposed an algorithm for solving the inverse source problem of a meromorphic function and apply their method to an electrical impedance tomography (EIT) problem.

El Badia [13] established a uniqueness result and a local Lipschitz stability estimate for an anisotropic elliptic equation, assuming that the sources are a linear combination of a finite number of monopoles and dipoles. The author also proposed a global Lipschitz stability estimate for dipolar sources.

Baratchart *et al.* [14] solved the inverse source problem by locating the singularities of a meromorphic function from the 2D boundary measurements using best rational or meromorphic approximations.

Chung and Chung [15] proposed an algorithm for detecting the combination of monopolar and multipolar point sources for elliptic equations in the 2D domain from the Neumann and Dirichlet boundary data.

Kandasmamy *et al.* [16] proposed a novel technique, called "analytic sensing", to estimate the positions and intensities of point sources in 2D for a Poisson's equation. Analytic sensing also used the reciprocity gap principle, but with a novel design of an analytic function which behaved like a sensor. The authors evaluated their estimation accuracy by Cramér-Rao lower bound.

Nara and Ando [17] proposed an algebraic method to localize the positions of multiple poles in meromorphic function field from an incomplete boundary. They investigated the accuracy of the algorithm for the open arc or the closed arc, and for the arc enclosing the poles or not enclosing the poles.

El Badia and Nara [18] established the uniqueness and local stability result for the inverse source problem of the Helmholtz equation in an interior domain, assuming the source is composed of multiple point sources.

Clerc *et al.* [19] applied best rational approximation techniques in the complex plane to EEG source localization and offered stability estimates.

Mdimagh and Ben Saad [20] identified the point sources in a scalar problem modeled by Helmholtz equation, using reciprocity gap principle and assuming the sources are harmonic in time. They proved local Lipschitz stability by two methods:

one was derived from the Gâteaux differentiability, and the other used particular test functions in the reciprocity gap functional.

In this dissertation, we study a harmonic function method for dipolar source reconstruction and apply the method to the real pain data. The outline of this dissertation is as follows. In chapter 2, “Preliminaries”, we review the fundamental solutions of the Laplacian equation and Sobolev space. In chapter 3, “The Inverse Source Problem”, we study the theory of inverse source problem, especially a harmonic function method for the dipolar source reconstruction. In chapter 4, “Error Estimate”, we provide the error estimate for the harmonic function method and compare our result with Chafik’s estimate. Then, in chapter 5, “Results”, we validate our method using both the computer-simulated data and the real pain data. Finally, in chapter 6, “Conclusions and Future Work”, we summarize the major findings of our research and discuss our future research plan.

CHAPTER 2

Preliminaries

2.1 Laplacian Equation

Laplacian equations and Poisson equations probably are the most important of all partial differential equations [21].

2.1.1 Introduction

Let u be the density of a physical quantity in equilibrium, V any smooth subregion within U, $\mathbf{F}$ the flux density, $\boldsymbol{\nu}$ the unit outer normal vector, then the flux of u through ∂V is zero:

$$\int_{\partial V} \mathbf{F} \cdot \boldsymbol{\nu} dS = 0.$$

By Gauss-Green Theorem, we have

$$\int_V \operatorname{div} \mathbf{F} dx = \int_V \nabla \cdot \mathbf{F} dx = \int_{\partial V} \mathbf{F} \cdot \boldsymbol{\nu} dS = 0,$$

which implies $\operatorname{div} \mathbf{F} = 0$ in U, since V is an arbitrary subregion.

Assume the flux density $\mathbf{F}$ is proportional to the gradient of the density u in the descending direction, i.e.,

$$\mathbf{F} = -a\nabla u, \quad a > 0.$$

Then,

$$0 = \operatorname{div} \mathbf{F} = \operatorname{div}(-a\nabla u) = \nabla \cdot (-a\nabla u) = -a\Delta u \implies \Delta u = 0.$$

Definition 1 (Laplacian equation and Poisson equation)**.** *Suppose $U \subset \mathbb{R}^n$ is a given open set, and $u = u(x), x \in U$ with $u : \overline{U} \to \mathbb{R}$ is an unknown function. Then,*

$$\Delta u = \sum_{j=1}^{n} \frac{\partial^2 u}{\partial x_j^2} = f$$

is a Laplacian equation if $f \equiv 0$, or a Poisson equation if $f \not\equiv 0$.

Definition 2 (Harmonic function)**.** *A C^2 function u satisfying $\Delta u = 0$ in Ω is called a harmonic function.*

2.1.2 Fundamental Solution

Theorem 1. *Laplacian equation $\Delta u = 0$ is rotation invariant; that is, if O is an orthonormal $n \times n$ matrix and we define*

$$v(x) := u(Ox), \quad x \in \mathbb{R}^n,$$

then $\Delta v = 0$.

Proof. Let $y = Ox$, i.e., $\begin{bmatrix} y_1 \\ y_2 \\ \vdots \\ y_n \end{bmatrix} = \begin{bmatrix} O_{11} & O_{12} & \cdots & O_{1n} \\ O_{21} & O_{22} & \cdots & O_{2n} \\ \vdots & & & \\ O_{n1} & O_{n2} & \cdots & O_{nn} \end{bmatrix} \begin{bmatrix} x_1 \\ x_2 \\ \vdots \\ x_n \end{bmatrix}$ where

$$y_j = O_{j1}x_1 + O_{j2}x_2 + \cdots + O_{ji}x_i + \cdots + O_{jn}x_n.$$

By chain rule,

$$\frac{\partial v}{\partial x_i} = \sum_{j=1}^{n} \frac{\partial u}{\partial y_j} \cdot \frac{\partial y_j}{\partial x_i} = \sum_{j=1}^{n} \frac{\partial u}{\partial y_j} \cdot O_{ji}.$$

O is orthonormal matrix $\implies O^T = O^{-1}$, i.e., $OO^T = O^T O = I$ where I is the identity matrix.

$$\sum_{i=1}^{n} O_{ki} O_{ji} = \sum_{i=1}^{n} O_{ki} O_{ij}^T = (OO^T)_{kj} = I_{kj} = \delta_{kj} = \begin{cases} 1, & k = j \\ 0, & k \neq j \end{cases}.$$

$$\begin{aligned}
\Delta v &= \sum_{i=1}^{n} \frac{\partial^2 v}{\partial x_i^2} = \sum_{i=1}^{n} \frac{\partial}{\partial x_i}\left(\frac{\partial v}{\partial x_i}\right) \\
&= \sum_{i=1}^{n} \frac{\partial}{\partial x_i}\left(\sum_{j=1}^{n} \frac{\partial u}{\partial y_j} \cdot O_{ji}\right) \\
&= \sum_{i=1}^{n}\sum_{k=1}^{n} \frac{\partial\left(\sum_{j=1}^{n} \frac{\partial u}{\partial y_j} \cdot O_{ji}\right)}{\partial y_k} \cdot \frac{\partial y_k}{\partial x_i} \\
&= \sum_{i=1}^{n}\sum_{k=1}^{n}\sum_{j=1}^{n} \frac{\partial^2 u}{\partial y_k \partial y_j} \cdot O_{ki} \cdot O_{ji} \\
&= \sum_{k=1}^{n}\sum_{j=1}^{n} \frac{\partial^2 u}{\partial y_k \partial y_j} \cdot \left(\sum_{i=1}^{n} O_{ki} \cdot O_{ji}\right) \\
&= \sum_{k=1}^{n}\sum_{j=1}^{n} \frac{\partial^2 u}{\partial y_k \partial y_j} \cdot \delta_{kj} \\
&= \sum_{k=1}^{n} \frac{\partial^2 u}{\partial y_k^2} = \Delta u = 0.
\end{aligned}$$

□

Assuming $u(x)$ is radially symmetric, we let

$$u(x) = v(r)$$

where $r = |x| = (x_1^2 + x_2^2 + \cdots + x_n^2)^{1/2}$.

$$\frac{\partial r}{\partial x_i} = \frac{1}{2}(x_1^2 + x_2^2 + \cdots + x_n^2)^{-1/2}(2x_i) = \frac{x_i}{r}, \quad r \neq 0.$$

$$\frac{\partial u}{\partial x_i} = \frac{\partial u}{\partial r} \cdot \frac{\partial r}{\partial x_i} = \frac{\partial v}{\partial r} \cdot \frac{x_i}{r} = v'(r)\frac{x_i}{r}.$$

$$
\begin{aligned}
\frac{\partial^2 u}{\partial x_i^2} &= \frac{\partial}{\partial x_i}\left(\frac{\partial u}{\partial x_i}\right) = \frac{\partial}{\partial x_i}\left(v'(r)\frac{x_i}{r}\right) \\
&= \frac{v'(r)}{r} + x_i \frac{\partial}{\partial x_i}\left(\frac{v'(r)}{r}\right) \\
&= \frac{v'(r)}{r} + x_i \frac{\partial}{\partial r}\left(\frac{v'(r)}{r}\right) \cdot \frac{\partial r}{\partial x_i} \\
&= \frac{v'(r)}{r} + \frac{x_i^2}{r} \cdot \frac{v''(r)r - v'(r)}{r^2} \\
&= \frac{v''(r)x_i^2}{r^2} + \frac{v'(r)}{r} - \frac{v'(r)x_i^2}{r^3}.
\end{aligned}
$$

$$
\begin{aligned}
\Delta u &= \sum_{i=1}^{n} \frac{\partial^2 u}{\partial x_i^2} \\
&= \sum_{i=1}^{n} \left[\frac{v''(r)x_i^2}{r^2} + \frac{v'(r)}{r} - \frac{v'(r)x_i^2}{r^3}\right] \\
&= v''(r) + \frac{v'(r)n}{r} - \frac{v'(r)}{r} \\
&= v''(r) + \frac{n-1}{r}v'(r) = 0.
\end{aligned}
$$

Let $w(r) = v'(r)$. Then, $w' + \frac{n-1}{r}w = 0 \implies \frac{dw}{dr} = \frac{1-n}{r}w \implies \frac{dw}{w} = \frac{1-n}{r}dr \implies \int \frac{dw}{w} = \int \frac{1-n}{r}dr \implies \ln|w| = (1-n)\ln|r| + C_1$ where C_1 is a constant $\implies |w| = C_2|r|^{1-n}$ where $C_2 > 0$ is a constant $\implies w = v'(r) = \frac{a}{r^{n-1}}$ where a is a constant.

When $n = 2$, we have $\frac{dv}{dr} = \frac{a}{r} \implies \int dv = \int \frac{a}{r}dr \implies v(r) = a\ln|r| + c = b\ln r + c$ where $b = a$ and c are constants.

When $n \geq 3$, we have $\frac{dv}{dr} = \frac{a}{r^{n-1}} \implies \int dv = \int ar^{1-n}dr \implies v(r) = a\frac{r^{2-n}}{2-n} + c = \frac{b}{r^{n-2}} + c$ where $b = \frac{a}{2-n}$ and c are constants.

Definition 3 (Fundamental solution of Laplacian equation)**.** *The function*

$$
\Phi(x) := \begin{cases} -\dfrac{1}{2\pi}\ln|x|, & n = 2 \\ \dfrac{1}{n(n-2)\alpha(n)} \cdot \dfrac{1}{|x|^{n-2}}, & n \geq 3 \end{cases}
$$

defined for $x \in \mathbb{R}^n, x \neq 0$, is the fundamental solution of Laplacian equation. $\alpha(n)$ denotes the volume of the unit ball in $\mathbb{R}^n$.

Theorem 2 (Solution of Poisson equation)**.** *Assume $f \in C_c^2(\mathbb{R}^n)$, i.e., f is twice continuously differentiable with compact support. Define*

$$u(x) = \int_{\mathbb{R}^n} \Phi(x-y)f(y)dy = \begin{cases} -\dfrac{1}{2\pi}\displaystyle\int_{\mathbb{R}^n} \ln(|x-y|)f(y)dy, & n = 2 \\ \dfrac{1}{n(n-2)\alpha(n)}\displaystyle\int_{\mathbb{R}^n} \dfrac{f(y)}{|x-y|^{n-2}}dy, & n \geq 3 \end{cases}.$$

Then, $u \in C^2(\mathbb{R}^n)$ and $-\Delta u = f$ in $\mathbb{R}^n$.

Proof.

1. To prove $u \in C^2(\mathbb{R}^n)$.
   $u(x) = \displaystyle\int_{\mathbb{R}^n} \Phi(x-y)f(y)dy$ is the convolution of the fundamental solution $\Phi(x)$ and the source $f(x)$. By the commutativity of convolution, we have

   $$u(x) = \int_{\mathbb{R}^n} \Phi(y)f(x-y)dy.$$

   Then,

   $$\frac{u(x+he_i)-u(x)}{h} = \int_{\mathbb{R}^n} \Phi(y)\frac{f(x+he_i-y)-f(x-y)}{h}dy$$

   where $h \neq 0$ and $e_i = (0, ..., 1, ..., 0)$ is the unit vector in $\mathbb{R}^n$ with 1 in the ith slot and 0 otherwise.

   Since $f \in C_c^2(\mathbb{R}^n)$,

   $$\frac{f(x+he_i-y)-f(x-y)}{h} \to \frac{\partial f}{\partial x_i}(x-y)$$

   uniformly in $\mathbb{R}^n$ as $h \to 0$. Then,

   $$\frac{\partial u}{\partial x_i}(x) = \int_{\mathbb{R}^n} \Phi(y)\frac{\partial f}{\partial x_i}(x-y)dy$$

and

$$\frac{\partial^2 u}{\partial x_i \partial x_j}(x) = \int_{\mathbb{R}^n} \Phi(y) \frac{\partial^2 f}{\partial x_i \partial x_j}(x-y)dy,$$

which is continuous. So, $u \in C^2(\mathbb{R}^n)$.

2. Since $\Phi(x)$ is singular at $x=0$, we calculate Δu separately.

$$\Delta u = \underbrace{\int_{B(0,\varepsilon)} \Phi(y)\Delta_x f(x-y)dy}_{I_\varepsilon} + \underbrace{\int_{\mathbb{R}^n - B(0,\varepsilon)} \Phi(y)\Delta_x f(x-y)dy}_{I_{\varepsilon'}},$$

where $B(0,\varepsilon)$ is a small ball centered at 0 with radius ε.

We know

$$\begin{aligned}
|I_\varepsilon| &= \left| \int_{B(0,\varepsilon)} \Phi(y)\Delta_x f(x-y)dy \right| \\
&\le \int_{B(0,\varepsilon)} |\Phi(y)| \cdot |\Delta_x f(x-y)|\, dy \\
&\le C\|D^2 f\|_{L^\infty(\mathbb{R}^n)} \int_{B(0,\varepsilon)} |\Phi(y)|dy \le \begin{cases} C\varepsilon^2 |\ln \varepsilon|, & n=2 \\ C\varepsilon^2, & n=3 \end{cases}
\end{aligned}$$

where $\|D^2 f\|_{L^\infty(\mathbb{R}^n)} = \max_{x\in\mathbb{R}^n, 1\le i,j\le n} |f_{x_i x_j}(x)|$.

When $n=2$, we have

$$\begin{aligned}
\int_{B(0,\varepsilon)} |\Phi(y)|dy &= \int_{B(0,\varepsilon)} \left| -\frac{1}{2\pi} \ln \sqrt{y_1^2 + y_2^2} \right| dy_1 dy_2 \\
&= \frac{1}{2\pi} \int_0^{2\pi} d\theta \int_0^\varepsilon |\ln r|\, r dr \\
&= \frac{\varepsilon^2}{2} |\ln \varepsilon| - \frac{\varepsilon^2}{4} \\
&\le \frac{\varepsilon^2}{2} |\ln \varepsilon|.
\end{aligned}$$

When $n = 3$, we have

$$\begin{aligned}\int_{B(0,\varepsilon)} |\Phi(y)| dy &= \int_{B(0,\varepsilon)} \frac{1}{n(n-2)\alpha(n)} \cdot \frac{1}{\sqrt{y_1^2 + y_2^2 + y_3^2}} dy_1 dy_2 dy_3 \\ &= \frac{1}{n(n-2)\alpha(n)} \int_0^{\pi} \sin\varphi d\varphi \int_0^{2\pi} d\theta \int_0^{\varepsilon} \frac{1}{r} r^2 dr \\ &= \frac{2\pi}{n(n-2)\alpha(n)} \varepsilon^2.\end{aligned}$$

By integration by parts [21] we have

$$\begin{aligned}I_{\varepsilon'} &= \int_{\mathbb{R}^n - B(0,\varepsilon)} \Phi(y) \Delta_x f(x-y) dy \\ &= \int_{\mathbb{R}^n - B(0,\varepsilon)} \Phi(y) \Delta_y f(x-y) dy \\ &= \underbrace{-\int_{\mathbb{R}^n - B(0,\varepsilon)} D\Phi(y) D_y f(x-y) dy}_{J_{\varepsilon'}} + \underbrace{\int_{\partial B(0,\varepsilon)} \Phi(y) \frac{\partial f}{\partial \nu}(x-y) dS(y)}_{J_\Gamma},\end{aligned}$$

where ν is the inward pointing unit normal along $\partial B(0,\varepsilon)$.

$$\begin{aligned}|J_\Gamma| &= \left| \int_{\partial B(0,\varepsilon)} \Phi(y) \frac{\partial f}{\partial \nu}(x-y) dS(y) \right| \\ &\le \int_{\partial B(0,\varepsilon)} |\Phi(y)| \cdot \left| \frac{\partial f}{\partial \nu}(x-y) \right| dS(y) \\ &\le \|Df\|_{L^\infty(\mathbb{R}^n)} \int_{\partial B(0,\varepsilon)} |\Phi(y)| \, dS(y) \le \begin{cases} C\varepsilon |\ln \varepsilon|, & n = 2 \\ C\varepsilon, & n = 3 \end{cases}.\end{aligned}$$

When $n = 2$, we have

$$\int_{\partial B(0,\varepsilon)} |\Phi(y)| \, dS(y) = \int_0^{2\pi} \left| -\frac{1}{2\pi} \ln \varepsilon \right| \varepsilon d\theta = \varepsilon |\ln \varepsilon|.$$

When $n = 3$, we have

$$\begin{aligned}
\int_{\partial B(0,\varepsilon)} |\Phi(y)|\, dS(y) &= \int_{\partial B(0,\varepsilon)} \left| \frac{1}{n(n-2)\alpha(n)} \cdot \frac{1}{|y|} \right| dS(y) \\
&= \frac{1}{n(n-2)\alpha(n)} \int_{\partial B(0,\varepsilon)} \frac{1}{\varepsilon} dS \\
&= \frac{1}{n(n-2)\alpha(n)} \cdot \frac{1}{\varepsilon} \cdot 4\pi\varepsilon^2 \\
&= \frac{4\pi}{n(n-2)\alpha(n)} \varepsilon.
\end{aligned}$$

By Gauss Theorem we have

$$\begin{aligned}
J_{\varepsilon'} &= -\int_{\mathbb{R}^n - B(0,\varepsilon)} D\Phi(y) D_y f(x-y) dy \\
&= \int_{\mathbb{R}^n - B(0,\varepsilon)} \underbrace{\Delta\Phi(y)}_{=0} f(x-y) dy - \int_{\mathbb{R}^n - B(0,\varepsilon)} \frac{\partial \Phi}{\partial \nu}(y) f(x-y) dS(y) \\
&= -\int_{\mathbb{R}^n - B(0,\varepsilon)} \frac{\partial \Phi}{\partial \nu}(y) f(x-y) dS(y) \\
&= -\frac{1}{n\alpha(n)\varepsilon^{n-1}} \int_{\mathbb{R}^n - B(0,\varepsilon)} f(x-y) dS(y) \\
&= -⨍_{\partial B(x,\varepsilon)} f(y) dS(y) \to -f(x) \text{ as } \varepsilon \to 0.
\end{aligned}$$

$\square$

Notice that the average of f over the ball $B(x,r)$ is

$$⨍_{B(x,r)} f dy := \frac{1}{\alpha(n) r^n} \int_{B(x,r)} f dy,$$

and the average of f over the spherical boundary $\partial B(x,r)$ is

$$⨍_{\partial B(x,r)} f dS := \frac{1}{n\alpha(n) r^{n-1}} \int_{\partial B(x,r)} f dS.$$

More generally, the average of f over set E is

$$⨍_E f d\mu := \frac{1}{\mu(E)} \int_E f d\mu,$$

provided $\mu(E) > 0$.

2.2 Sobolev Space

Banach spaces and Hilbert spaces play a central role in functional analysis [22], while Sobolev space is of fundamental importance for the formulation of finite element methods [23].

Definition 4 (Banach space)**.** *A real (complex) normed linear space that is complete is called a Banach space.*

Definition 5 (Hilbert space)**.** *A nonempty set H is called a Hilbert space if H is a complex linear vector space, together with a complex-valued function $(\cdot,\cdot)$ from $H \times H$ into $\mathbb{C}$ having the following properties:*

1. $(x,x) \geq 0$, *and* $(x,x) = 0$ *if and only if* $x = 0$;
2. $(x+y,z) = (x,z) + (y,z)$ *for all* x, y, z *in* H;
3. $(\lambda x, y) = \lambda(x,y)$ *for all* x, y *in* H *and* $\lambda \in \mathbb{C}$;
4. $(x,y) = \overline{(y,x)}$ *for all* x, y *in* H;
5. *if* $\{x_n\} \subset H$, $\lim_{n,m\to\infty}(x_n - x_m, x_n - x_m) = 0$, *then there is an element* $x \in H$ *such that* $\lim_{n\to\infty}(x_n - x, x_n - x) = 0$.

Definition 6 (Sobolev space)**.** *Let Ω be any open subset of $\mathbb{R}^n$. We denote by $H^{m,p}(\Omega)$ or $H^{m/p}(\Omega)$ the space of functions $u \in L^p(\Omega)$ such that $\left(\frac{\partial}{\partial x}\right)^\alpha u \in L^p(\Omega)$ for all $\alpha = (\alpha_1, ..., \alpha_n) \in \mathbb{Z}_+^n$, $|\alpha| = \alpha_1 + \cdots + \alpha_n \leq m$, $1 \leq p \leq \infty$.*

$H^{m,p}(\Omega)$ is equipped with the norm

$$\|u\|_{m,p} = \left\{ \sum_{|\alpha|\leq m} \left\| \left(\frac{\partial}{\partial x}\right)^\alpha u \right\|_{L^p(\Omega)}^p \right\}^{1/p}, \quad 1 \leq p < \infty,$$

$$\|u\|_{m,\infty} = \sup_{|\alpha|\leq m} \left\| \left(\frac{\partial}{\partial x}\right)^\alpha u \right\|_{L^\infty(\Omega)}.$$

If $p = 2$, one usually writes $H^m(\Omega)$ instead of $H^{m,2}(\Omega)$.

Definition 7 (Sobolev space of order s)**.** *$H^s(\mathbb{R}^n)$ or H^s is the Sobolev space of order $s \in \mathbb{R}$ in $\mathbb{R}^n$, i.e., the space of tempered distributions u in $\mathbb{R}^n$ whose Fourier transform $\hat{u}$ is a measurable function such that*

$$\|u\|_s = \left(\frac{1}{(2\pi)^n} \int_{\mathbb{R}^n} |\hat{u}(\xi)|^2 (1 + |\xi|^2)^s d\xi \right)^{1/2} < \infty,$$

equipped with the Hilbert space structure defined by the norm $\| \cdot \|_s$.

CHAPTER 3

The Inverse Source Problem

3.1 Mathematical Model of EEG Problem

The electric field $\mathbf{E}$ is the negative gradient of the potential u.

$$\mathbf{E} = -\nabla u.$$

The quasi-static approximation means all time derivatives in the equation are set to zero. By quasi-static approximation of Maxwell equation $\nabla \times \mathbf{H} - \dfrac{\partial \mathbf{D}}{\partial t} = \mathbf{J}$, we have

$$\nabla \times \mathbf{H} = \mathbf{J}$$

where $\mathbf{H}$ is the magnetizing field, $\mathbf{J}$ is the total current density, and $\mathbf{D}$ is the displacement field.

Since the divergence of a curl is always zero, we have

$$\nabla \cdot (\nabla \times \mathbf{H}) = \nabla \cdot \mathbf{J} = 0.$$

EEG problem can be modeled by a Poisson equation.

$$\begin{aligned} -\nabla \cdot (\sigma \nabla u) &= \nabla \cdot (\sigma \mathbf{E}) \\ &= \nabla \cdot (\mathbf{J} - \mathbf{J}^p) \\ &= \underbrace{\nabla \cdot \mathbf{J}}_{=0} - \nabla \cdot \mathbf{J}^p \\ &= -\nabla \cdot \mathbf{J}^p \\ &= F, \end{aligned}$$

where σ is the conductivity, $\mathbf{J}^p$ is the primary current density, and F is the source term.

3.2 Source Model

If we assume the source is composed of a finite number of point charges, then by linear combination, we have

$$F = \sum_{k=1}^{m} q_k \delta(\mathbf{r} - \mathbf{r}_k), \tag{3.1}$$

where m is the number of point charges, q_k are values of charges, and $\mathbf{r}_k$ are the locations of the point charges.

If we assume the source is composed of a finite number of dipoles, we have

$$F = -\sum_{k=1}^{m} \mathbf{p}_k \cdot \nabla \delta(\mathbf{r} - \mathbf{r}_k).$$

where m is the number of dipoles, $\mathbf{p}_k$ are the moments (or strengths) of the dipoles, and $\mathbf{r}_k$ are the centers of dipoles.

3.3 The Harmonic Function Method of Identifying Dipolar Sources

The dipolar source reconstruction problem can be viewed as a Poisson problem.

$$\Delta u = \sum_{k=1}^{m} \mathbf{p}_k \cdot \nabla \delta(\mathbf{r} - \mathbf{r}_k) \text{ in } \Omega, \tag{3.2}$$

$$u = f \text{ on } \Gamma, \tag{3.3}$$

$$\frac{\partial u}{\partial \nu} = \varphi \text{ on } \Gamma, \tag{3.4}$$

where f and φ are known, and ν is the outer unit normal vector.

We will use the concept of reciprocity gap functional [24]:

$$\begin{aligned} R(v) &= \left\langle \frac{\partial u}{\partial \nu}, v \right\rangle_{H^{1/2}(\Gamma), H^{-1/2}(\Gamma)} - \left\langle u, \frac{\partial v}{\partial \nu} \right\rangle_{H^{1/2}(\Gamma), H^{-1/2}(\Gamma)} \\ &= \langle \varphi, v \rangle_{H^{1/2}(\Gamma), H^{-1/2}(\Gamma)} - \left\langle f, \frac{\partial v}{\partial \nu} \right\rangle_{H^{1/2}(\Gamma), H^{-1/2}(\Gamma)}, \end{aligned} \tag{3.5}$$

where v is a harmonic function in Ω:

$$v \in H(\Omega) = \{ w \in H^1(\Omega) \mid \Delta w = 0 \}. \tag{3.6}$$

By Green's formula, we have

$$R(v) = -\sum_{k=1}^{m} \mathbf{p}_k \cdot \nabla v(\mathbf{r} - \mathbf{r}_k), \forall v \in H(\Omega). \tag{3.7}$$

Let m be the number of dipoles in the brain. Assume $m \leq M$ in our problem, i.e., there is an upper bound for the number of dipoles.

Let us consider the harmonic polynomials

$$v_j(x, y) = (x + iy)^j, \quad j \in \mathbb{N}.$$

Then, in 2D case

$$\begin{aligned}
R(v_j) &= -\sum_{k=1}^{m} \mathbf{p}_k \cdot \nabla v_j(\mathbf{r}_k) \\
&= -\sum_{k=1}^{m} \begin{bmatrix} p_{k1} \\ p_{k2} \end{bmatrix} \cdot \nabla (x_k + iy_k)^j \\
&= -\sum_{k=1}^{m} \begin{bmatrix} p_{k1} \\ p_{k2} \end{bmatrix} \cdot \begin{bmatrix} \frac{\partial}{\partial x}(x+iy)^j \\ \frac{\partial}{\partial y}(x+iy)^j \end{bmatrix}_{x=x_k, y=y_k} \\
&= -\sum_{k=1}^{m} \begin{bmatrix} p_{k1} \\ p_{k2} \end{bmatrix} \cdot \begin{bmatrix} j(x_k+iy_k)^{j-1} \cdot 1 \\ j(x_k+iy_k)^{j-1} \cdot i \end{bmatrix} \\
&= -\sum_{k=1}^{m} \begin{bmatrix} p_{k1} \\ p_{k2} \end{bmatrix} \cdot \begin{bmatrix} 1 \\ i \end{bmatrix} j(x_k+iy_k)^{j-1} \\
&= -j \sum_{k=1}^{m} (p_{k1} + ip_{k2})(x_k + iy_k)^{j-1}.
\end{aligned}$$

We define

$$\beta_j := \frac{R(v_j)}{-j} = \sum_{k=1}^{M} (p_{k1} + ip_{k2})(x_k + iy_k)^{j-1}, \quad j = 1, 2, ..., 2M-1. \tag{3.8}$$

Let

$$\eta_j = \begin{bmatrix} \beta_j \\ \beta_{j+1} \\ \vdots \\ \beta_{j+M-1} \end{bmatrix} \in \mathbb{C}^M, \quad 1 \le j \le M, \tag{3.9}$$

and

$$Z_i = \begin{bmatrix} \eta_i, \eta_{i+1}, ..., \eta_{i+M-1} \end{bmatrix} = \begin{bmatrix} \beta_i & \beta_{i+1} & \cdots & \beta_{i+M-1} \\ \beta_{i+1} & \beta_{i+2} & \cdots & \beta_{i+M} \\ \vdots & & & \\ \beta_{i+M-1} & \beta_{i+M} & \cdots & \beta_{i+2M-2} \end{bmatrix}, \quad i \in \mathbb{N}.$$

Then,

$$Z_1 = \left[\eta_1, \eta_2, ..., \eta_M\right] = \begin{bmatrix} \beta_1 & \beta_2 & \cdots & \beta_M \\ \beta_2 & \beta_3 & \cdots & \beta_{M+1} \\ \vdots & & & \\ \beta_M & \beta_{M+1} & \cdots & \beta_{2M-1} \end{bmatrix}.$$

The number m of dipoles is estimated as the rank of Z_1.

Now we can reduce the size of the matrix by recalculating β_j and η_j with M replaced by m. Then, the m vectors $\eta_1, ..., \eta_m$ are independent.

To get the estimates of the positions we need to construct an $m \times m$ matrix T such that $\eta_{j+1} = T\eta_j, j = 1, ..., m$. Then,

$$[\eta_2, ..., \eta_{m+1}] = T[\eta_1, ..., \eta_m].$$

So,

$$\begin{aligned} T &= [\eta_2, ..., \eta_{m+1}][\eta_1, ..., \eta_m]^{-1} \\ &= \begin{bmatrix} \beta_2 & \beta_3 & \cdots & \beta_{m+1} \\ \beta_3 & \beta_4 & \cdots & \beta_{m+2} \\ \vdots & & & \\ \beta_{m+1} & \beta_{m+2} & \cdots & \beta_{2m} \end{bmatrix} \begin{bmatrix} \beta_1 & \beta_2 & \cdots & \beta_m \\ \beta_2 & \beta_3 & \cdots & \beta_{m+1} \\ \vdots & & & \\ \beta_m & \beta_{m+1} & \cdots & \beta_{2m-1} \end{bmatrix}^{-1} \\ &= Z_2 Z_1^{-1}. \end{aligned}$$

The positions of dipoles are estimated as the eigenvalues of T.

Why the eigenvalues of T are the positions of dipoles? Let us first look at an example $\eta_2 = T\eta_1$.

$$
\begin{aligned}
T\eta_1 &= T \begin{bmatrix} \beta_1 \\ \beta_2 \\ \vdots \\ \beta_m \end{bmatrix} = T \begin{bmatrix} p_1 + p_2 + \cdots + p_m \\ p_1 S_1 + p_2 S_2 + \cdots + p_m S_m \\ \vdots \\ p_1 S_1^{m-1} + p_2 S_2^{m-1} + \cdots + p_m S_m^{m-1} \end{bmatrix} \\
&= p_1 T \begin{bmatrix} 1 \\ S_1 \\ \vdots \\ S_1^{m-1} \end{bmatrix} + p_2 T \begin{bmatrix} 1 \\ S_2 \\ \vdots \\ S_2^{m-1} \end{bmatrix} + \cdots + p_m T \begin{bmatrix} 1 \\ S_m \\ \vdots \\ S_m^{m-1} \end{bmatrix}.
\end{aligned}
$$

$$
\begin{aligned}
\eta_2 &= \begin{bmatrix} \beta_2 \\ \beta_3 \\ \vdots \\ \beta_{m+1} \end{bmatrix} = \begin{bmatrix} p_1 S_1 + p_2 S_2 + \cdots + p_m S_m \\ p_1 S_1^2 + p_2 S_2^2 + \cdots + p_m S_m^2 \\ \vdots \\ p_1 S_1^m + p_2 S_2^m + \cdots + p_m S_m^m \end{bmatrix} \\
&= p_1 S_1 \begin{bmatrix} 1 \\ S_1 \\ \vdots \\ S_1^{m-1} \end{bmatrix} + p_2 S_2 \begin{bmatrix} 1 \\ S_2 \\ \vdots \\ S_2^{m-1} \end{bmatrix} + \cdots + p_m S_m \begin{bmatrix} 1 \\ S_m \\ \vdots \\ S_m^{m-1} \end{bmatrix}.
\end{aligned}
$$

Since $\begin{bmatrix} 1 \\ S_1 \\ \vdots \\ S_1^{m-1} \end{bmatrix}, \begin{bmatrix} 1 \\ S_2 \\ \vdots \\ S_2^{m-1} \end{bmatrix}, ..., \begin{bmatrix} 1 \\ S_m \\ \vdots \\ S_m^{m-1} \end{bmatrix}$ are independent and the results are similar for $\eta_{j+1} = T\eta_j, j = 1, 2, ..., m$, we know $S_1, S_2, ..., S_m$ are just the eigenvalues of T.

Now the question is how to get T. Only η_1 and η_2 are not enough to determine T because vectors have no inverse. So, we use the redundant information to construct the matrices Z_1 and Z_2 such that $T = Z_2 Z_1^{-1}$, where Z_1 is invertible because $\eta_1, ..., \eta_m$ are independent.

To estimate the moments of dipoles we will write Eq. (3.8) in matrix form. Notice that now we use m instead of M.

$$\begin{bmatrix} \beta_1 \\ \beta_2 \\ \vdots \\ \beta_m \end{bmatrix} = \begin{bmatrix} S_1^0 & S_2^0 & \cdots & S_m^0 \\ S_1^1 & S_2^1 & \cdots & S_m^1 \\ \vdots & & & \\ S_1^{m-1} & S_2^{m-1} & \cdots & S_m^{m-1} \end{bmatrix} \begin{bmatrix} p_1 \\ p_2 \\ \vdots \\ p_m \end{bmatrix}, \tag{3.10}$$

where $p_k = p_{k1} + ip_{k2}$ is the moment and $S_k = x_k + iy_k$ is the position.

We can write Eq. (3.10) in matrix form

$$\mathbf{b} = \mathbf{S}\mathbf{p}, \tag{3.11}$$

where $\mathbf{b} = \begin{bmatrix} \beta_1 \\ \beta_2 \\ \vdots \\ \beta_m \end{bmatrix}$, $\mathbf{S} = \begin{bmatrix} S_1^0 & S_2^0 & \cdots & S_m^0 \\ S_1^1 & S_2^1 & \cdots & S_m^1 \\ \vdots & & & \\ S_1^{m-1} & S_2^{m-1} & \cdots & S_m^{m-1} \end{bmatrix}$, and $\mathbf{p} = \begin{bmatrix} p_1 \\ p_2 \\ \vdots \\ p_m \end{bmatrix}$. Then, the moments of dipoles in 2D are estimated as

$$\mathbf{p} = \mathbf{S}^{-1}\mathbf{b}. \tag{3.12}$$

3.4 Optimization of linear operator

Eq. (3.12) works in the ideal case of no noise. In reality, due to the noise in the measurements and in the sources, we need find a linear operator $\mathbf{L}$ to estimate the moments, i.e.,

$$\tilde{\mathbf{p}} = \mathbf{L}\mathbf{b} \tag{3.13}$$

where $\tilde{\mathbf{p}}$ represents the estimates of the moments, and $\mathbf{b}$ represents the quantities obtained from the measurements.

Considering the noise accompanied in the measurements, we rewrite Eq. (3.11) as

$$\mathbf{b} = \mathbf{S}\mathbf{p} + \mathbf{n},$$

where $\mathbf{n}$ is a random vector of mean 0. Let $\mathbf{N}$ be the covariance matrix of $\mathbf{n}$. Also, assume that $\tilde{\mathbf{p}}$ is normally distributed with mean $\mathbf{p}$ and its covariance matrix is $\mathbf{P}$.

Using multiple measurements and the statistical estimation theory we can find the linear operator $\mathbf{L}$ which minimizes the expected difference $Err_{\mathbf{L}}$ between the estimated moments $\tilde{\mathbf{p}}$ and the exact moments $\mathbf{p}$.

$$\begin{aligned}
Err_{\mathbf{L}} &= \langle \|\tilde{\mathbf{p}} - \mathbf{p}\|^2 \rangle \\
&= \langle \|\mathbf{L}\mathbf{b} - \mathbf{p}\|^2 \rangle \\
&= \langle \|\mathbf{L}(\mathbf{S}\mathbf{p} + \mathbf{n}) - \mathbf{p}\|^2 \rangle \\
&= \langle \|(\mathbf{L}\mathbf{S} - \mathbf{I})\mathbf{p} + \mathbf{L}\mathbf{n}\|^2 \rangle \\
&= \langle \|\mathbf{M}\mathbf{p} + \mathbf{L}\mathbf{n}\|^2 \rangle \quad (\text{where } \mathbf{M} = \mathbf{L}\mathbf{S} - \mathbf{I}) \\
&= \langle \|\mathbf{M}\mathbf{p}\|^2 \rangle + \langle \|\mathbf{L}\mathbf{n}\|^2 \rangle \quad (\text{by independence of } \mathbf{p} \text{ and } \mathbf{n}) \\
&= Tr(\mathbf{M}\mathbf{P}\mathbf{M}^T) + Tr(\mathbf{L}\mathbf{N}\mathbf{L}^T).
\end{aligned}$$

Setting the gradient of $Err_{\mathbf{L}}$ to 0 and solving for $\mathbf{L}$, we get the optimal linear operator

$$\mathbf{L} = \mathbf{P}\mathbf{S}^T(\mathbf{S}\mathbf{P}\mathbf{S}^T + \mathbf{N})^{-1}. \tag{3.14}$$

Then, by Eq. (3.13) we get the best estimates of the moments.

3.5 Uniqueness of solutions

Theorem 3 (Uniqueness of solutions)**.** *Let $u_i, i = 1, 2$ be the solutions of the problems*

$$-\nabla \cdot (\sigma \nabla u_i) = \sum_{k=1}^{m_i} \mathbf{p}_k^{(i)} \cdot \nabla \delta_{S_k^{(i)}} \ \mathit{in}\ \Omega,$$

$$\frac{\partial u_i}{\partial \nu} = \varphi \ \mathit{on}\ \Gamma,$$

such that

$$u_1 = u_2 \ \mathit{on}\ \Gamma,$$

then

$$m_1 = m_2 = m,$$

$$\mathbf{p}_k^{(1)} = \mathbf{p}_k^{(2)}, \forall k = 1, 2, ..., m,$$

$$S_k^{(1)} = S_k^{(2)}, \forall k = 1, 2, ..., m.$$

Proof. We give a sketch of the proof.

1. Use the transmission conditions to rewrite PDE for the innermost layer.

$$\begin{aligned}
-\Delta w &= \sum_{k=1}^{m_2} \mathbf{p}_k^{(2)} \cdot \delta_{S_k^{(2)}} - \sum_{k=1}^{m_1} \mathbf{p}_k^{(1)} \cdot \delta_{S_k^{(1)}} \text{ in } \Omega, \\
w &= 0 \text{ on } \partial\Omega, \\
\frac{\partial w}{\partial \nu} &= 0 \text{ on } \partial\Omega.
\end{aligned}$$

2. The solution of Poisson equation is the convolution of the fundamental solution of Laplace equation and the source function.

$$w(x) = \frac{1}{2\pi}\left[\sum_{k=1}^{m_2} \frac{\mathbf{p}_k \cdot (x - S_k)}{\left|x - S_k^{(2)}\right|^2} - \sum_{k=1}^{m_1} \frac{\mathbf{p}_k \cdot (x - S_k)}{\left|x - S_k^{(1)}\right|^2}\right], n = 2.$$

$$w(x) = \frac{-1}{4\pi}\left[\sum_{k=1}^{m_2} \frac{\mathbf{p}_k \cdot (x - S_k)}{\left|x - S_k^{(2)}\right|^3} - \sum_{k=1}^{m_1} \frac{\mathbf{p}_k \cdot (x - S_k)}{\left|x - S_k^{(1)}\right|^3}\right], n = 3.$$

□

CHAPTER 4

Error Estimate

As EEG imaging data are typically noisy, especially determining the rank of a near singular matrix is very unstable, the error of the numerical reconstruction method needs to be studied. Chafik *et al.* [10, 9] proposed that when the norms of the perturbations ($g = \tilde{f} - f, h = \tilde{\varphi} - \varphi$) are small in $H^{1/2} \times H^{-1/2}$, there exist $a > 0$ and $b > 0$ such that $\forall k = 1, 2, ..., m$,

$$\|\tilde{S}_k - S_k\|_2 \leq \frac{m(1-R^m)}{d^{m-1}(1-R)} \max\left\{ \binom{m-1}{j} R^j, 0 \leq j \leq m-1 \right\} \left(a\|g\|_{H^{1/2}(\Gamma)} + b\|h\|_{H^{-1/2}(\Gamma)} \right),$$

where $S_k = x_k + iy_k$ is the exact position of the kth dipole, $\tilde{S}_k = \tilde{x}_k + i\tilde{y}_k$ is the estimated position of the kth dipole, d is the minimal distance between S_k and $\tilde{S}_k$, and $R \neq 1$ is a real number bigger than the norm of any point on Γ. However, the analysis is not given by Chafik *et al.*

We derive a new form of error estimate

$$\begin{aligned} & \|T - \tilde{T}\|_\infty \\ \leq\ & 2m \left(\|\varphi\|_2 R^{2m} \sqrt{2\pi R} + \|f\|_2 R^{2m} \sqrt{2\pi R} \right) \left(\frac{m! m^{m-1} p_{max}^{m-1} R^{m(m-1)}}{p_{min}^m d^{m(m-1)}} \right) \\ & + 2m^2 \left(\|\varphi\|_2 R^{2m} \sqrt{2\pi R} + \|f\|_2 R^{2m} \sqrt{2\pi R} \right)^2 \left(\frac{m! m^{m-1} p_{max}^{m-1} R^{m(m-1)}}{p_{min}^m d^{m(m-1)}} \right)^2, \end{aligned}$$

and give a mathematical proof. A simple numerical example is provided that the error estimate of Chafik *et al.* may not be valid for some cases.

4.1 Introduction

Error estimate is crucial for numerical applications [20].

Researchers have done error estimate for inverse problems related to electric filed models. Alessandrini *et al.* [25, 26], and Bellout et al. [19] have dealt with stability for an inverse conductivity problem.

Bellout et al. [19] introduced the notion of local Lipschitz stability, which are widely used in cracks, boundary recovery and Robin's coefficient [20-22].

Assuming that the poles are well separated and their respective strengths are large enough, Cannon et al. [23] obtained a logarithm-type stability estimate for the 2D case problem of identifying dense masses in the earth from gravimetry data taken at the surface or in the air.

Vessella [8] proved Lipschitz stability results in the problem of determining locations and strengths of point sources in 3-D Euclidean spaces from the measurements of potentials on the boundary.

El Badia and El Hajj [27] provided the Hölder stability estimates for some inverse point-wise source problems.

El Badia and El Hajj [28] showed the Hölder stability estimates for the inverse source problem of Helmholtz's equation in 3-D case.

Abdelaziz *et al.* designed direct algorithms for multipolar sources reconstruction [29] and for solving some inverse source problems in 2D elliptic equations [30].

El Badia *et al.* [31] made Lipschitz stability estimates for an inverse monopolar source problem of an elliptic equation from interior measurements in anisotropic media.

El Badia *et al.* [32] investigated an inverse source problem of the time harmonic Maxwell equations and provided a Hölder stability estimate.

Mdimagh and Saad [20] used two methods to get the local Lipschitz stability results of the point sources in 2D and 3D cases. One method used Gâteaux differentiability and the other method used the reciprocity gap concept [8] with particular test functions.

4.2 Error Estimates of Positions

We define

$$Z_i = \begin{bmatrix} \beta_i & \beta_{i+1} & \cdots & \beta_{i+m-1} \\ \beta_{i+1} & \beta_{i+2} & \cdots & \beta_{i+m} \\ \vdots & & & \\ \beta_{i+m-1} & \beta_{i+m} & \cdots & \beta_{i+2m-2} \end{bmatrix}, \quad i \in \mathbb{N}.$$

Then,

$$Z_1 = \begin{bmatrix} \beta_1 & \beta_2 & \cdots & \beta_m \\ \beta_2 & \beta_3 & \cdots & \beta_{m+1} \\ \vdots & & & \\ \beta_m & \beta_{m+1} & \cdots & \beta_{2m-1} \end{bmatrix}.$$

where

$$\beta_j = \sum_{k=1}^{m} p_k S_k^{j-1} = \sum_{k=1}^{m} (p_{k1} + ip_{k2})(x_k + iy_k)^{j-1}, \quad j = 1, 2, ..., 2m-1.$$

$$
\det(Z_1) = \begin{vmatrix} \beta_1 & \beta_2 & \cdots & \beta_m \\ \beta_2 & \beta_3 & \cdots & \beta_{m+1} \\ \vdots & & & \\ \beta_m & \beta_{m+1} & \cdots & \beta_{2m-1} \end{vmatrix} = \begin{vmatrix} \sum p_k & \sum p_k S_k & \cdots & \sum p_k S_k^{m-1} \\ \sum p_k S_k & \sum p_k S_k^2 & \cdots & \sum p_k S_k^m \\ \vdots & & & \\ \sum p_k S_k^{m-1} & \sum p_k S_k^m & \cdots & \sum p_k S_k^{2m-2} \end{vmatrix}
$$

$$
= \sum_{m_1 \neq m_2 \neq \cdots \neq m_m} \tau(m_1, m_2, ..., m_m) \cdot p_{m_1} p_{m_2} \cdots p_{m_m} \begin{vmatrix} 1 & S_{m_2} & \cdots & S_{m_m}^{m-1} \\ S_{m_1} & S_{m_2}^2 & \cdots & S_{m_m}^m \\ \vdots & & & \\ S_{m_1}^{m-1} & S_{m_2}^m & \cdots & S_{m_m}^{2m-2} \end{vmatrix}
$$

$$
= \sum_{m_1 \neq m_2 \neq \cdots \neq m_m} \tau(m_1, m_2, ..., m_m) \cdot p_{m_1} p_{m_2} \cdots p_{m_m} \begin{vmatrix} 1 & 1 & \cdots & 1 \\ S_{m_1} & S_{m_2} & \cdots & S_{m_m} \\ \vdots & & & \\ S_{m_1}^{m-1} & S_{m_2}^{m-1} & \cdots & S_{m_m}^{m-1} \end{vmatrix} S_{m_1}^0 S_{m_2}^1 \cdots S_{m_m}^{m-1}
$$

$$
= p_1 p_2 \cdots p_m \begin{vmatrix} 1 & 1 & \cdots & 1 \\ S_{m_1} & S_{m_2} & \cdots & S_{m_m} \\ \vdots & & & \\ S_{m_1}^{m-1} & S_{m_2}^{m-1} & \cdots & S_{m_m}^{m-1} \end{vmatrix} \left(\sum_{m_1 \neq m_2 \neq \cdots \neq m_m} \tau(m_1, m_2, ..., m_m) \cdot S_{m_1}^0 S_{m_2}^1 \cdots S_{m_m}^{m-1} \right)
$$

$$
= p_1 p_2 \cdots p_m \begin{vmatrix} 1 & 1 & \cdots & 1 \\ S_{m_1} & S_{m_2} & \cdots & S_{m_m} \\ \vdots & & & \\ S_{m_1}^{m-1} & S_{m_2}^{m-1} & \cdots & S_{m_m}^{m-1} \end{vmatrix} \cdot \begin{vmatrix} 1 & 1 & \cdots & 1 \\ S_{m_1} & S_{m_2} & \cdots & S_{m_m} \\ \vdots & & & \\ S_{m_1}^{m-1} & S_{m_2}^{m-1} & \cdots & S_{m_m}^{m-1} \end{vmatrix}
$$

$$
= p_1 p_2 \cdots p_m \prod_{1 \le i < j \le m} (S_i - S_j)^2.
$$

Here, $(m_1, m_2, ..., m_m)$ is any permutation of $(1, 2, ..., m)$ and $\tau(m_1, m_2, ..., m_m)$ is the sign determined by the permutation.

The maximum absolute row sum norm is defined by

$$\|A\|_\infty = \max_i \sum_j |a_{ij}|,$$

where A is a matrix. When A is a vector, $\|A\|_\infty = \max_i |a_i|$.

In the following proof we will use an important inequality:

$$\|a(x)b(x) - a(y)b(y)\|_\infty \le \|a(x) - a(y)\|_\infty \cdot \|b(x)\|_\infty + \|b(x) - b(y)\|_\infty \cdot \|a(x)\|_\infty$$

where $a(x)$ and $b(x)$ can be scalar, vector, or matrix.

By Cauchy-Schwarz inequality, we have

$$\begin{aligned}
R(v_j) &= \langle \varphi, v_j \rangle - \left\langle f, \frac{\partial v_j}{\partial \nu} \right\rangle \\
&= \int_\Gamma \varphi \cdot v_j ds - \int_\Gamma f \cdot \frac{\partial v_j}{\partial \nu} ds \\
&= \int_\Gamma \varphi \cdot (x+iy)^j ds - \int_\Gamma f \cdot \frac{\partial (x+iy)^j}{\partial \nu} ds \\
&\le \left(\int_\Gamma \varphi^2 ds \right)^{1/2} \left(\int_\Gamma (x+iy)^{2j} ds \right)^{1/2} + \left(\int_\Gamma f^2 ds \right)^{1/2} \left(\int_\Gamma \left(\frac{\partial (x+iy)^j}{\partial \nu} \right)^2 ds \right)^{1/2} \\
&\le \left(\int_\Gamma \varphi^2 ds \right)^{1/2} R^j \sqrt{2\pi R} + \left(\int_\Gamma f^2 ds \right)^{1/2} j R^{j-1} \sqrt{2\pi R} \\
&\le j \|\varphi\|_2 R^j \sqrt{2\pi R} + j \|f\|_2 R^{j-1} \sqrt{2\pi R}.
\end{aligned}$$

$$\begin{aligned}
|\beta_j| &= \left| \frac{R(v_j)}{-j} \right| \\
&\le \|\varphi\|_2 R^j \sqrt{2\pi R} + \|f\|_2 R^{j-1} \sqrt{2\pi R} \\
&\le \|\varphi\|_2 R^{2m} \sqrt{2\pi R} + \|f\|_2 R^{2m} \sqrt{2\pi R}
\end{aligned}$$

where $R > 1$.

Let

$$T = Z_2 Z_1^{-1} = Z_2 \frac{\operatorname{adj}(Z_1)}{\det(Z_1)}$$

where $Z_1 = \begin{bmatrix} \beta_1 & \beta_2 & \cdots & \beta_m \\ \beta_2 & \beta_3 & \cdots & \beta_{m+1} \\ \vdots & & & \\ \beta_m & \beta_{m+1} & \cdots & \beta_{2m-1} \end{bmatrix}$ and $Z_2 = \begin{bmatrix} \beta_2 & \beta_3 & \cdots & \beta_{m+1} \\ \beta_3 & \beta_4 & \cdots & \beta_{m+2} \\ \vdots & & & \\ \beta_{m+1} & \beta_{m+2} & \cdots & \beta_{2m} \end{bmatrix}$.

We can view $R(v_j)$ as the measurement obtained by the "detector" v_j, while β_j is just a constant multiple of $R(v_j)$. So, β_j is still a measurement of another form, which contains the information about the moment and the position of the dipole source. Since Z_1 and Z_2 are constructed by different measurements β_j, T is also a matrix of measurements.

Assume T is the measurements without noise, and $\tilde{T}$ is the measurements with noise. Then,

$$\begin{aligned} \|T - \tilde{T}\|_\infty &= \|Z_2 Z_1^{-1} - \tilde{Z}_2 \tilde{Z}_1^{-1}\|_\infty \\ &\leq \|Z_2 - \tilde{Z}_2\|_\infty \|Z_1^{-1}\|_\infty + \|Z_1^{-1} - \tilde{Z}_1^{-1}\|_\infty \|Z_2\|_\infty. \end{aligned}$$

We will analyse the four norms in the above inequality one by one.

$$\|Z_2 - \tilde{Z}_2\|_\infty \leq m\|\varphi - \tilde{\varphi}\|_2 R^{2m}\sqrt{2\pi R} + m\|f - \tilde{f}\|_2 R^{2m}\sqrt{2\pi R}.$$

To find $\|Z_1^{-1}\|_\infty$ we need to estimate $\|\operatorname{adj}(Z_1)\|_\infty$. We first observe the results for $m = 3$ and $m = 4$, then generalize the results to the arbitrary m.

If $Z_1 = \begin{bmatrix} \beta_1 & \beta_2 & \beta_3 \\ \beta_2 & \beta_3 & \beta_4 \\ \beta_3 & \beta_4 & \beta_5 \end{bmatrix}$, then the absolute value of the first element of $\operatorname{adj}(Z_1)$ would be

$$
\begin{aligned}
\operatorname{abs}\left(\begin{vmatrix} \beta_3 & \beta_4 \\ \beta_4 & \beta_5 \end{vmatrix}\right) &= |\beta_3\beta_5 - \beta_4^2| \leq |\beta_3| \cdot |\beta_5| + |\beta_4^2| \\
&= (p_1S_1^2 + p_2S_2^2 + p_3S_3^2)(p_1S_1^4 + p_2S_2^4 + p_3S_3^4) + (p_1S_1^3 + p_2S_2^3 + p_3S_3^3)^2 \\
&\leq (3p_{max}R^2)(3p_{max}R^4) + (3p_{max}R^3)^2 = 2(3p_{max}R^3)^2 \\
&= (3-1)!3^{3-1}p_{max}^{3-1}R^{3(3-1)} \\
&=: \max\left(\operatorname{abs}\left(\begin{vmatrix} \beta_3 & \beta_4 \\ \beta_4 & \beta_5 \end{vmatrix}\right)\right).
\end{aligned}
$$

Then,

$$
\begin{aligned}
& \|\operatorname{adj}(Z_1)\|_\infty \\
\leq\ & \max\left(\operatorname{abs}\left(\begin{vmatrix} \beta_3 & \beta_4 \\ \beta_4 & \beta_5 \end{vmatrix}\right)\right) + \max\left(\operatorname{abs}\left(\begin{vmatrix} \beta_2 & \beta_4 \\ \beta_3 & \beta_5 \end{vmatrix}\right)\right) + \max\left(\operatorname{abs}\left(\begin{vmatrix} \beta_2 & \beta_3 \\ \beta_3 & \beta_4 \end{vmatrix}\right)\right) \\
\leq\ & 3 \cdot \max\left(\operatorname{abs}\left(\begin{vmatrix} \beta_3 & \beta_4 \\ \beta_4 & \beta_5 \end{vmatrix}\right)\right) \\
=\ & 3 \cdot (3-1)!3^{3-1}p_{max}^{3-1}R^{3(3-1)} \\
=\ & 3!3^{3-1}p_{max}^{3-1}R^{3(3-1)}.
\end{aligned}
$$

If $Z_1 = \begin{bmatrix} \beta_1 & \beta_2 & \beta_3 & \beta_4 \\ \beta_2 & \beta_3 & \beta_4 & \beta_5 \\ \beta_3 & \beta_4 & \beta_5 & \beta_6 \\ \beta_4 & \beta_5 & \beta_6 & \beta_7 \end{bmatrix}$, then the absolute value of the first element of $\mathrm{adj}(Z_1)$ would be

$$\begin{aligned}
\mathrm{abs}\left(\begin{vmatrix} \beta_3 & \beta_4 & \beta_5 \\ \beta_4 & \beta_5 & \beta_6 \\ \beta_5 & \beta_6 & \beta_7 \end{vmatrix}\right) &= |\beta_3\beta_5\beta_7 + 2\beta_4\beta_5\beta_6 - \beta_5^3 - \beta_3\beta_6^2 - \beta_4^2\beta_7| \\
&\leq |\beta_3\beta_5\beta_7| + |2\beta_4\beta_5\beta_6| + |\beta_5^3| + |\beta_3\beta_6^2| + |\beta_4^2\beta_7| \\
&\leq 6\max(|\beta_5^3|) \\
&= 6\max(p_1S_1^4 + p_2S_2^4 + p_3S_3^4 + p_4S_4^4)^3 \leq 6(4p_{max}R^4)^3 \\
&= (4-1)!4^{4-1}p_{max}^{4-1}R^{4(4-1)} \\
&=: \max\left(\mathrm{abs}\left(\begin{vmatrix} \beta_3 & \beta_4 & \beta_5 \\ \beta_4 & \beta_5 & \beta_6 \\ \beta_5 & \beta_6 & \beta_7 \end{vmatrix}\right)\right).
\end{aligned}$$

Then,

$$
\begin{aligned}
&\|\operatorname{adj}(Z_1)\|_\infty \\
\leq\ & \max\left(\operatorname{abs}\left(\begin{vmatrix}\beta_3 & \beta_4 & \beta_5\\ \beta_4 & \beta_5 & \beta_6\\ \beta_5 & \beta_6 & \beta_7\end{vmatrix}\right)\right) + \max\left(\operatorname{abs}\left(\begin{vmatrix}\beta_2 & \beta_4 & \beta_5\\ \beta_3 & \beta_5 & \beta_6\\ \beta_4 & \beta_6 & \beta_7\end{vmatrix}\right)\right) \\
& + \max\left(\operatorname{abs}\left(\begin{vmatrix}\beta_2 & \beta_3 & \beta_5\\ \beta_3 & \beta_4 & \beta_6\\ \beta_4 & \beta_5 & \beta_7\end{vmatrix}\right)\right) + \max\left(\operatorname{abs}\left(\begin{vmatrix}\beta_2 & \beta_3 & \beta_4\\ \beta_3 & \beta_4 & \beta_5\\ \beta_4 & \beta_5 & \beta_6\end{vmatrix}\right)\right) \\
\leq\ & 4\cdot\max\left(\operatorname{abs}\left(\begin{vmatrix}\beta_3 & \beta_4 & \beta_5\\ \beta_4 & \beta_5 & \beta_6\\ \beta_5 & \beta_6 & \beta_7\end{vmatrix}\right)\right) \\
\leq\ & 4\cdot(4-1)!4^{4-1}p_{max}^{4-1}R^{4(4-1)} \\
=\ & 4!4^{4-1}p_{max}^{4-1}R^{4(4-1)}.
\end{aligned}
$$

Assume when $m = n-1$, we have

$$
\operatorname{abs}\left(\begin{vmatrix}\beta_3 & \beta_4 & \cdots & \beta_{n+1}\\ \beta_4 & \beta_5 & \cdots & \beta_{n+2}\\ \vdots & & & \\ \beta_{n+1} & \beta_{n+2} & \cdots & \beta_{2n-1}\end{vmatrix}\right) \leq (n-1)!n^{n-1}p_{max}^{n-1}R^{n(n-1)}.
$$

In fact, this inequality is also true for other minors with matrix size $(n-1)\times(n-1)$.

Then, when $m = n$ we have

$$
\begin{aligned}
& \text{abs}\left(\begin{vmatrix} \beta_3 & \beta_4 & \cdots & \beta_{n+1} & \beta_{n+2} \\ \beta_4 & \beta_5 & \cdots & \beta_{n+2} & \beta_{n+3} \\ \vdots & & & & \\ \beta_{n+1} & \beta_{n+2} & \cdots & \beta_{2n-1} & \beta_{2n} \\ \beta_{n+2} & \beta_{n+3} & \cdots & \beta_{2n} & \beta_{2n+1} \end{vmatrix}\right) \\
\leq \quad & \max|\beta_{2n+1}| \cdot \max\left(\text{abs}\begin{vmatrix} \beta_3 & \beta_4 & \cdots & \beta_{n+1} \\ \beta_4 & \beta_5 & \cdots & \beta_{n+2} \\ \vdots & & & \\ \beta_{n+1} & \beta_{n+2} & \cdots & \beta_{2n-1} \end{vmatrix}\right) + \cdots \\
& + \max|\beta_{n+2}| \cdot \max\left(\text{abs}\begin{vmatrix} \beta_4 & \beta_5 & \cdots & \beta_{n+2} \\ \beta_5 & \beta_6 & \cdots & \beta_{n+3} \\ \vdots & & & \\ \beta_{n+2} & \beta_{n+3} & \cdots & \beta_{2n} \end{vmatrix}\right) \\
\leq \quad & n \cdot \max|\beta_{2n+1}| \cdot \max\left(\text{abs}\begin{vmatrix} \beta_3 & \beta_4 & \cdots & \beta_{n+1} \\ \beta_4 & \beta_5 & \cdots & \beta_{n+2} \\ \vdots & & & \\ \beta_{n+1} & \beta_{n+2} & \cdots & \beta_{2n-1} \end{vmatrix}\right) \\
\leq \quad & n \cdot \max|p_1 S_1^{2n} + p_2 S_2^{2n} + \cdots + p_n S_n^{2n}| \cdot (n-1)! n^{n-1} p_{max}^{n-1} R^{n(n-1)} \\
\leq \quad & n \cdot n p_{max} R^{2n} \cdot (n-1)! n^{n-1} p_{max}^{n-1} R^{n^2-n)} \\
= \quad & n! n^n p_{max}^n R^{(n+1)n} \\
\leq \quad & n!(n+1)^n p_{max}^n R^{(n+1)n}.
\end{aligned}
$$

Then, for any m we have

$$
\begin{aligned}
\|\operatorname{adj}(Z_1)\|_\infty &= \left\| \operatorname{adj}\left(\begin{bmatrix} \beta_1 & \beta_2 & \cdots & \beta_{m-1} & \beta_m \\ \beta_2 & \beta_3 & \cdots & \beta_m & \beta_{m+1} \\ \vdots & & & & \\ \beta_{m-1} & \beta_m & \cdots & \beta_{2m-3} & \beta_{2m-2} \\ \beta_m & \beta_{m+1} & \cdots & \beta_{2m-2} & \beta_{2m-1} \end{bmatrix} \right) \right\|_\infty \\
&\leq \max\left(\operatorname{abs} \begin{vmatrix} \beta_3 & \beta_4 & \cdots & \beta_{m+1} \\ \beta_4 & \beta_5 & \cdots & \beta_{m+2} \\ \vdots & & & \\ \beta_{m+1} & \beta_{m+2} & \cdots & \beta_{2m-1} \end{vmatrix} \right) + \cdots + \max\left(\operatorname{abs} \begin{vmatrix} \beta_2 & \beta_3 & \cdots & \beta_m \\ \beta_3 & \beta_4 & \cdots & \beta_{m+1} \\ \vdots & & & \\ \beta_m & \beta_{m+1} & \cdots & \beta_{2m-2} \end{vmatrix} \right) \\
&\leq m \cdot \max\left(\operatorname{abs} \begin{vmatrix} \beta_3 & \beta_4 & \cdots & \beta_{m+1} \\ \beta_4 & \beta_5 & \cdots & \beta_{m+2} \\ \vdots & & & \\ \beta_{m+1} & \beta_{m+2} & \cdots & \beta_{2m-1} \end{vmatrix} \right) \\
&= m \cdot (m-1)! m^{m-1} p_{max}^{m-1} R^{m(m-1)} \\
&= m! m^{m-1} p_{max}^{m-1} R^{m(m-1)}.
\end{aligned}
$$

Thus,

$$
\begin{aligned}
\|Z_1^{-1}\|_\infty &= \left\| \frac{\operatorname{adj}(Z_1)}{\det(Z_1)} \right\|_\infty \\
&\leq \frac{m! m^{m-1} p_{max}^{m-1} R^{m(m-1)}}{p_1 p_2 \cdots p_m \prod_{1 \leq i < j \leq m} (S_i - S_j)^2} \\
&\leq \frac{m! m^{m-1} p_{max}^{m-1} R^{m(m-1)}}{p_{min}^m d^{m(m-1)}}
\end{aligned}
$$

where d is the smallest distance between any two points.

Notice that

$$Z_1(Z_1^{-1} - \tilde{Z}_1^{-1}) + (Z_1 - \tilde{Z}_1)\tilde{Z}_1^{-1} = 0.$$

$$Z_1^{-1} - \tilde{Z}_1^{-1} = -Z_1^{-1}(Z_1 - \tilde{Z}_1)\tilde{Z}_1^{-1}.$$

$$\begin{aligned}
& \|Z_1^{-1} - \tilde{Z}_1^{-1}\|_\infty \\
\leq\ & \|Z_1^{-1}\|_\infty \cdot \|Z_1 - \tilde{Z}_1\|_\infty \cdot \|\tilde{Z}_1^{-1}\|_\infty \\
\leq\ & \left(\frac{m! m^{m-1} p_{max}^{m-1} R^{m(m-1)}}{p_{min}^m d^{m(m-1)}}\right)^2 \cdot \left(m\|\varphi - \tilde{\varphi}\|_2 R^{2m}\sqrt{2\pi R} + m\|f - \tilde{f}\|_2 R^{2m}\sqrt{2\pi R}\right).
\end{aligned}$$

Based on the above results, we have

$$\begin{aligned}
& \|T - \tilde{T}\|_\infty \\
\leq\ & \|Z_2 - \tilde{Z}_2\|_\infty \|Z_1^{-1}\|_\infty + \|Z_1^{-1} - \tilde{Z}_1^{-1}\|_\infty \|Z_2\|_\infty. \\
\leq\ & \left(m\|\varphi - \tilde{\varphi}\|_2 R^{2m}\sqrt{2\pi R} + m\|f - \tilde{f}\|_2 R^{2m}\sqrt{2\pi R}\right)\left(\frac{m! m^{m-1} p_{max}^{m-1} R^{m(m-1)}}{p_{min}^m d^{m(m-1)}}\right) \\
& + \left(\frac{m! m^{m-1} p_{max}^{m-1} R^{m(m-1)}}{p_{min}^m d^{m(m-1)}}\right)^2 \cdot \left(m\|\varphi - \tilde{\varphi}\|_2 R^{2m}\sqrt{2\pi R} + m\|f - \tilde{f}\|_2 R^{2m}\sqrt{2\pi R}\right) \\
& \cdot \left(m\|\varphi\|_2 R^{2m}\sqrt{2\pi R} + m\|f\|_2 R^{2m}\sqrt{2\pi R}\right) \\
\leq\ & 2m\left(\|\varphi\|_2 R^{2m}\sqrt{2\pi R} + \|f\|_2 R^{2m}\sqrt{2\pi R}\right)\left(\frac{m! m^{m-1} p_{max}^{m-1} R^{m(m-1)}}{p_{min}^m d^{m(m-1)}}\right) \\
& + 2m^2\left(\|\varphi\|_2 R^{2m}\sqrt{2\pi R} + \|f\|_2 R^{2m}\sqrt{2\pi R}\right)^2 \left(\frac{m! m^{m-1} p_{max}^{m-1} R^{m(m-1)}}{p_{min}^m d^{m(m-1)}}\right)^2 \\
\leq\ & E + E^2
\end{aligned}$$

where

$$E = 2mR^{2m}\sqrt{2\pi R}\left(\|f\|_2 + \|\varphi\|_2\right)\left(\frac{m! m^{m-1} p_{max}^{m-1} R^{m(m-1)}}{p_{min}^m d^{m(m-1)}}\right).$$

When $0 < E < 1$, the error in the position estimate is mainly controlled by E; when $E > 1$, the error in the position estimate is mainly controlled by E^2.

CHAPTER 5

Results

5.1 Numerical simulation for 2D

Let Ω be a circular disk centered at the origin and of radius $r = 1$. Then, the numerical implementation can be simplified as follow.

$$\frac{\partial v_j}{\partial \nu} = \frac{\partial (x+iy)^j}{\partial r} = \frac{\partial \left(re^{i\theta}\right)^j}{\partial r} = jr^{j-1}e^{i\theta j} = \frac{jr^j e^{i\theta j}}{r} = \frac{jv_j}{r}.$$

$$\begin{aligned}
R(v_j) &= -\left\langle f, \frac{\partial v_j}{\partial \nu} \right\rangle \\
&= -\int_\Gamma f \cdot \frac{\partial v_j}{\partial \nu} d\Gamma \\
&= -\int_0^{2\pi} f \cdot \frac{jv_j}{r} \cdot r d\theta \\
&= -j \int_0^{2\pi} f \cdot v_j d\theta \\
&= -j \int_0^{2\pi} f \cdot \left(re^{i\theta}\right)^j d\theta,
\end{aligned}$$

where f is a function of θ on the boundary. We don't know the explicit form of f, but we can measure as many points as possible on the boundary to get enough discretized function values of f. Then, the above integral can be approximated by a Riemann sum.

The measurable values we want to use in the following are

$$\beta_j = -\frac{R(v_j)}{j} = \int_0^{2\pi} f \cdot \left(re^{i\theta}\right)^j \, d\theta.$$

The Romberg algorithm is used to calculate the integral numerically.

We compare the efficacy of the harmonic function method in dipolar source reconstruction when the perturbation level is $0, 0.001, 0.01, 0.1$ and the number of dipoles is $1, 2, 3, 4, 5$. It is shown that as the perturbation level increases, the reconstruction error increases.

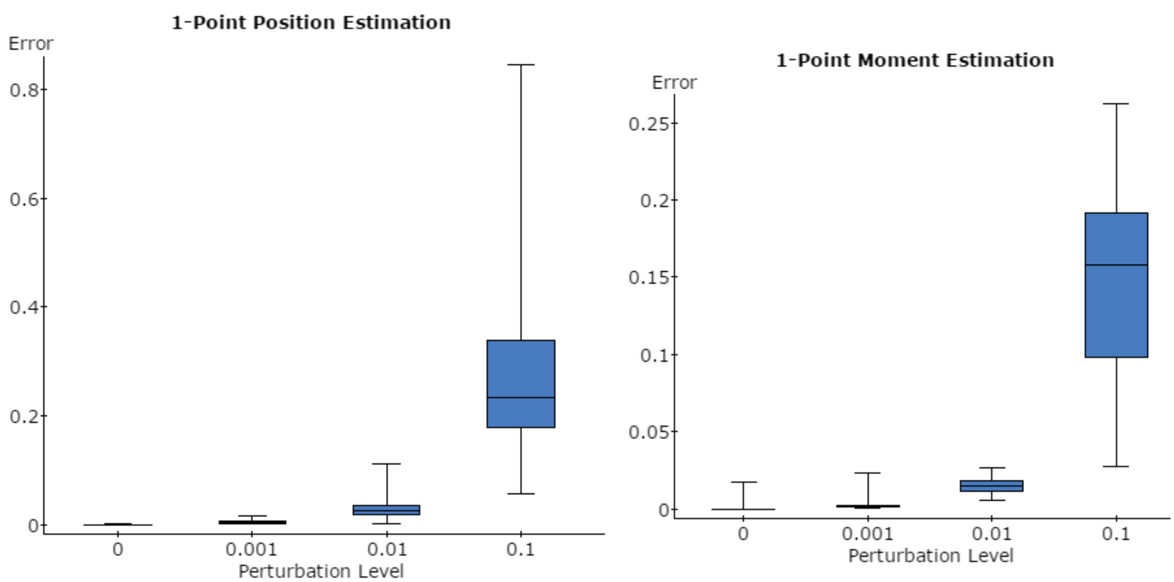

Figure 5.1. The effect of the perturbation level on the reconstruction error of 1 dipole. As the perturbation level increases, the reconstruction error increases. Here, the perturbation means adding noise to the exact measurement. If the perturbation level is σ, then the perturbed measurement is the exact measurement times $(1 \pm \sigma)$, where plus or minus signs are randomly assigned to each channel. Here, the error is defined as the sum of position errors.

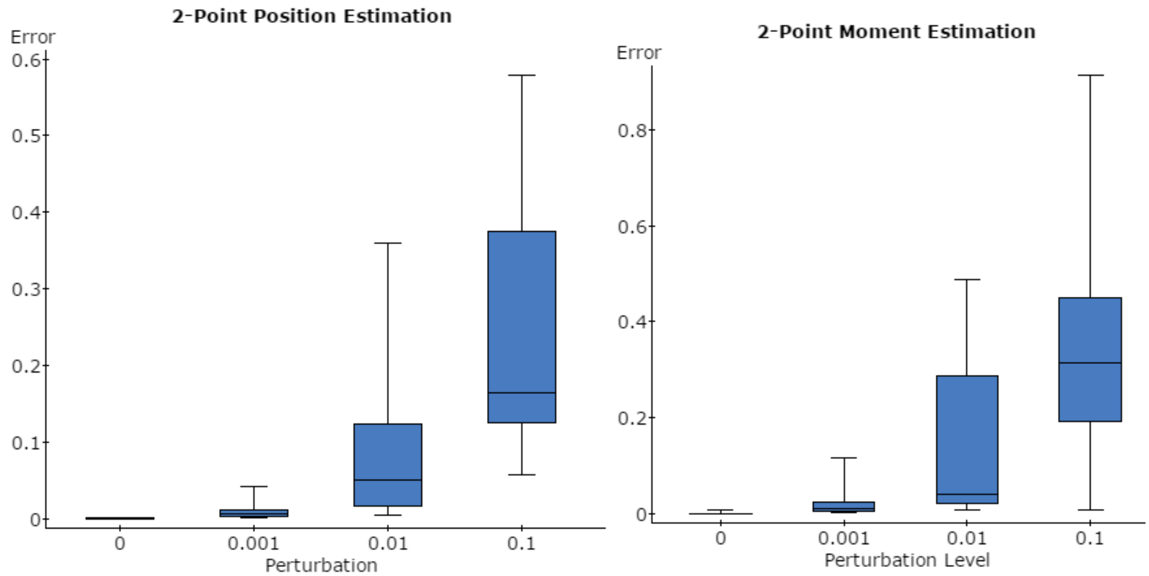

Figure 5.2. The effect of the perturbation level on the reconstruction error of 2 dipoles. As the perturbation level increases, the reconstruction error increases. Here, the perturbation means adding noise to the exact measurement. If the perturbation level is σ, then the perturbed measurement is the exact measurement times $(1 \pm \sigma)$, where plus or minus signs are randomly assigned to each channel. Here, the error is defined as the sum of position errors.

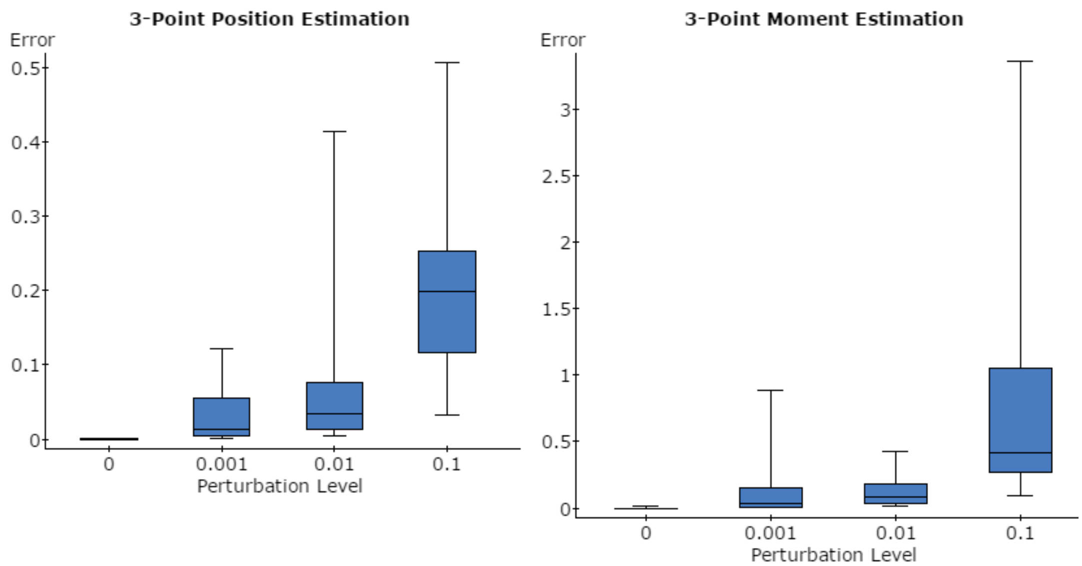

Figure 5.3. The effect of the perturbation level on the reconstruction error of 3 dipoles. As the perturbation level increases, the reconstruction error increases. Here, the perturbation means adding noise to the exact measurement. If the perturbation level is σ, then the perturbed measurement is the exact measurement times $(1 \pm \sigma)$, where plus or minus signs are randomly assigned to each channel. Here, the error is defined as the sum of position errors.

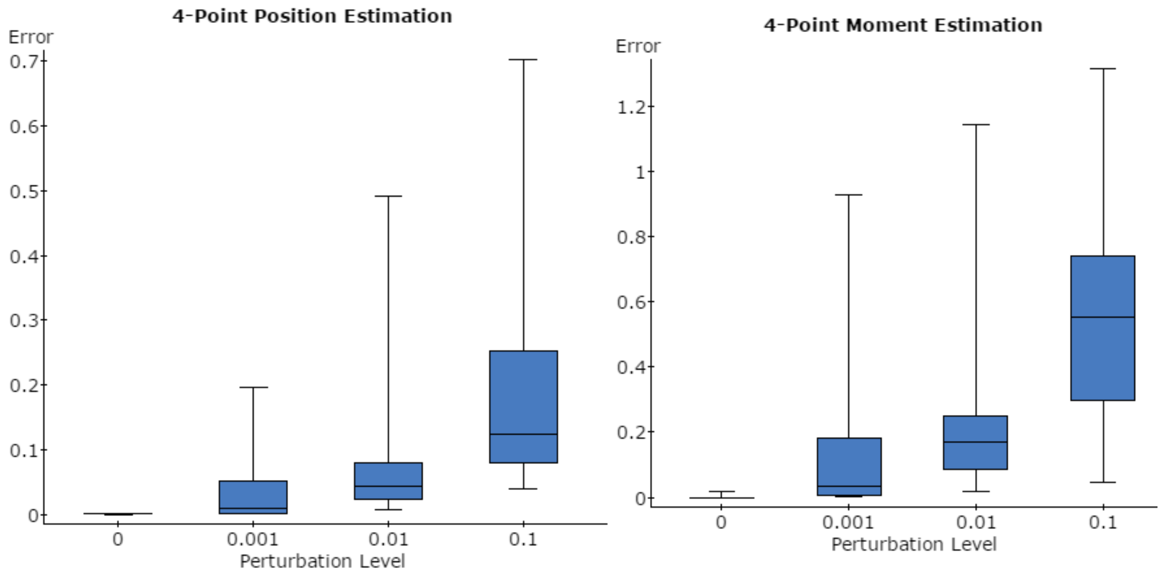

Figure 5.4. The effect of the perturbation level on the reconstruction error of 4 dipoles. As the perturbation level increases, the reconstruction error increases. Here, the perturbation means adding noise to the exact measurement. If the perturbation level is σ, then the perturbed measurement is the exact measurement times $(1 \pm \sigma)$, where plus or minus signs are randomly assigned to each channel. Here, the error is defined as the sum of position errors.

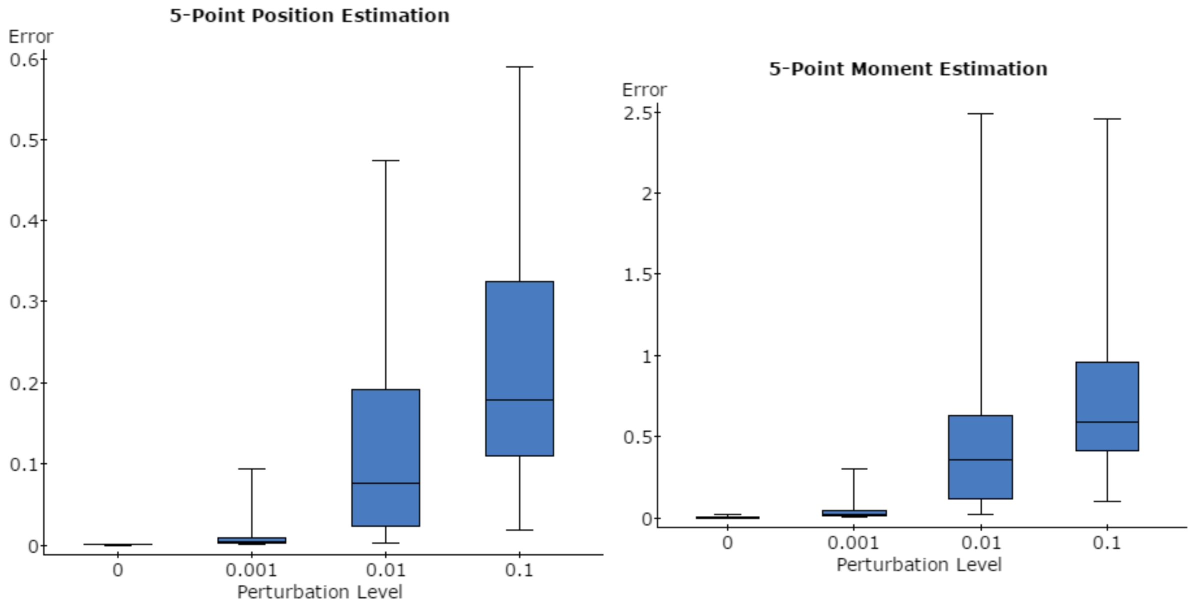

Figure 5.5. The effect of the perturbation level on the reconstruction error of 5 dipoles. As the perturbation level increases, the reconstruction error increases. Here, the perturbation means adding noise to the exact measurement. If the perturbation level is σ, then the perturbed measurement is the exact measurement times $(1 \pm \sigma)$, where plus or minus signs are randomly assigned to each channel. Here, the error is defined as the sum of position errors.

In the following we show the results of source estimation, assuming there are 3 dipolar sources ($m = 3$).

- Dipole 1. Position $(0.3, -0.3)$ and moment $(0, 1)$.
- Dipole 2. Position $(0.6, 0.2)$ and moment $(1, 1)$.
- Dipole 3. Position $(-0.5, 0.4)$ and moment $(2, 2)$.

In the graphs we use a small circle and a red line segment to indicate the true value, and use a cross sign and a green line segment to indicate the reconstructed values.

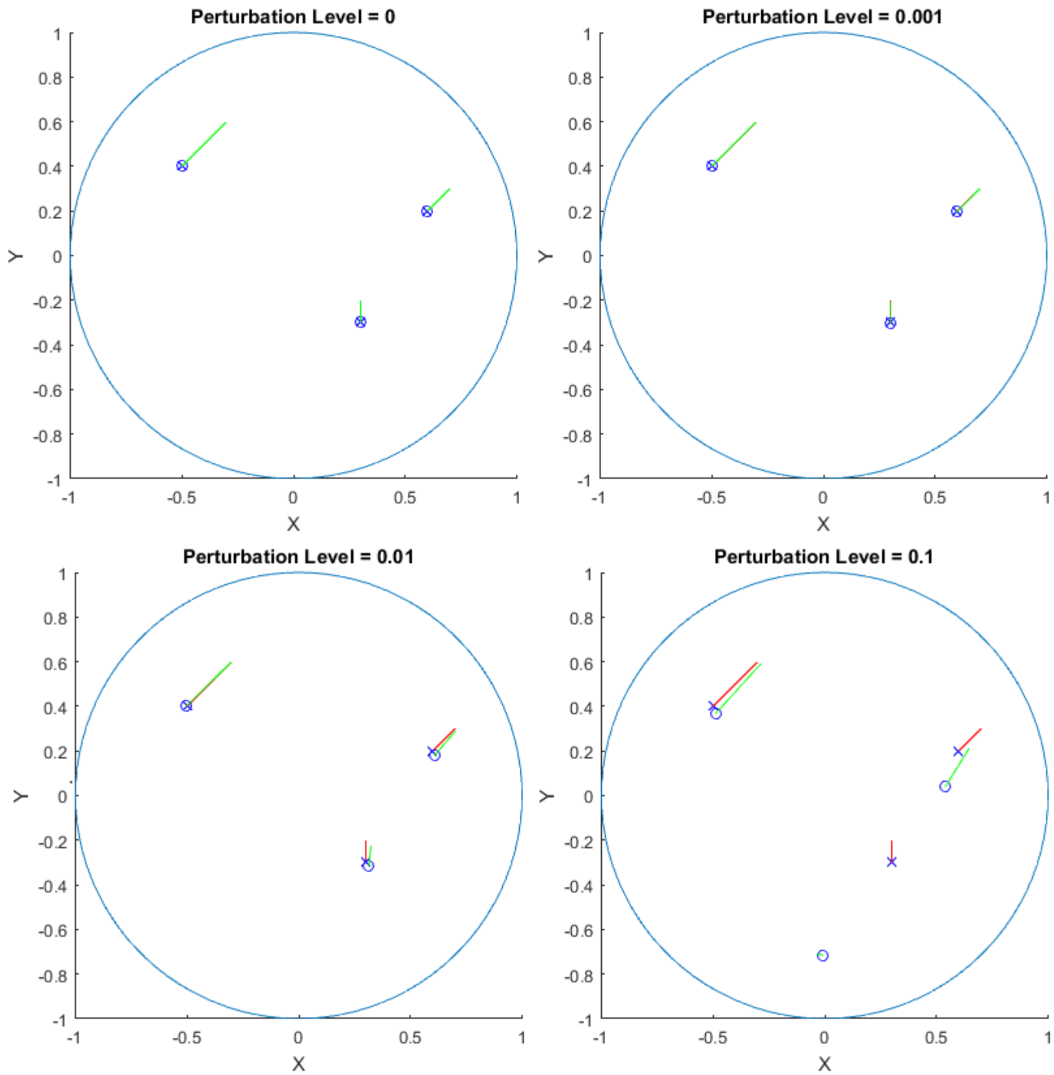

Figure 5.6. The effect of the perturbation level on the reconstruction error of 3 dipoles. As the perturbation level increases, the reconstruction error increases.

From error estimates we know that as the distance between two dipoles gets closer, the reconstruction error for the positions of dipoles gets larger (see Table 5.1 and Fig. 5.7). This is verified by the numerical simulations.

We randomly assign two dipoles with fixed distance, say 0.1, in the unit disk, then reconstruct their positions. We fix the noise level for all experiments at $\sigma = 0.001$.

Let $d_i, i = 1, 2$ be the distance between the ith exact dipole and the ith estimated dipole, and d_{max} be the largest d.

We repeat the experiment 10 times and show their performance on average over different dipole distances.

The above experiment also provides a numerical example to show that the estimate provided by Chafik *et al.* may be wrong in some cases.

When the number of dipoles is $m = 2$, Chafik's estimate is bounded by $\dfrac{C}{d}$, while our estimate is bounded by $\dfrac{C}{d^2}$ where C is a constant and d is the smallest distance between two dipoles. That is, when the distance is halved, the estimate error will be amplified by 2 in Chafik's estimate and by 4 in our estimate.

From the data simulation, we see that

$$\frac{0.05}{0.03} = 1.67 < \frac{0.7429}{0.3084} = 2.41 < 1.67^2 = 2.79.$$

$$\frac{0.10}{0.05} = 2 < \frac{0.3084}{0.1200} = 2.57 < 2^2 = 4.$$

$$\frac{0.10}{0.03} = 3.33 < \frac{0.7429}{0.1200} = 6.19 < 3.33^2 = 11.09.$$

For example, when the distance between the two dipoles is reduced from 0.10 to 0.05, by Chafik's estimate the error should be amplified by 2, but in fact, the error is amplified by 2.57, which is bounded by 4 in our estimate. Similarly, the other two comparisons of ratio also show that Chafik's estimate may be wrong in some cases.

Exact Dipole Distance	**Reconstructed Dipole Distance**
0.03	0.7429
0.05	0.3084
0.10	0.1200

Table 5.1. The effect of dipole distance on the reconstruction error. As two dipoles get closer, the mean reconstruction error in the positions of the dipoles gets larger, which is consistent with the result in the error estimate.

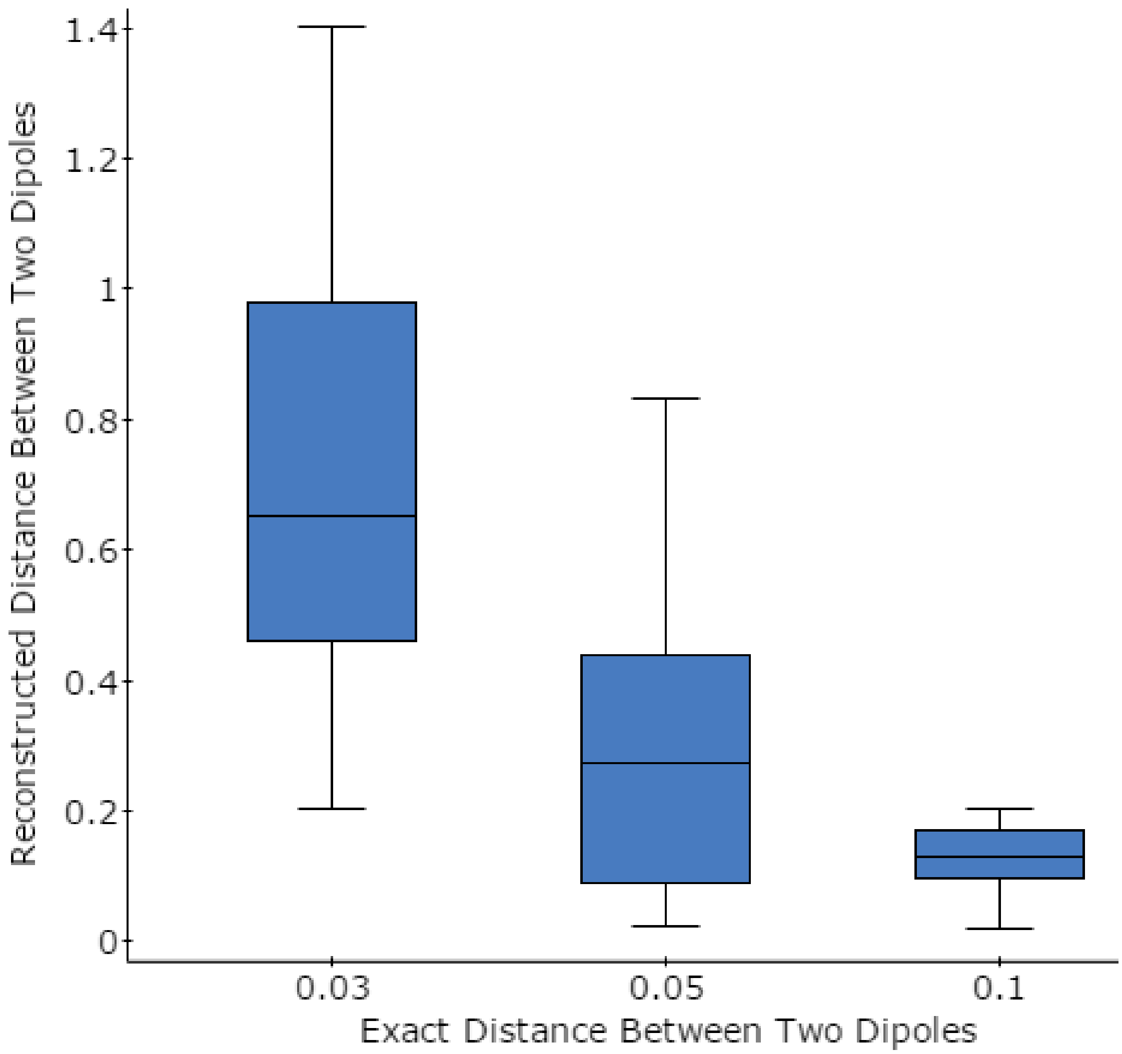

Figure 5.7. The effect of dipole distance on the reconstruction error. As two dipoles get closer, the reconstruction error in the positions of the dipoles gets larger, which is consistent with the theoretical analysis in the error estimate. When $d_{exact} = 0.10$, $\overline{d_{est}} = 0.1200$; when $d_{exact} = 0.05$, $\overline{d_{est}} = 0.3084$; when $d_{exact} = 0.03$, $\overline{d_{est}} = 0.7429$.

5.2 Application in EEG data of Pain

Pain quantification is essential for pain relief. In clinical situations the pain is assessed by the patients' reporting, which is subjective and inaccurate. For example, children or patients with communication disabilities are unable to express their pain effectively. So, methods or equipment for objective and accurate assessment of pain are needed.

We obtained a set of human pain EEG data from Dr. Yuanbo Peng's lab at UT Arlington. The experiment is operated in the following way.

The subject wears an EasyCap-M1 74-electrode helmet [33] (see Fig. 5.8), where only 66 electrodes were used in our experiments, and the other 8 electrodes ($F_{pz}, F_9, F_{10}, P_9, P_{10}, O_9, O_{10}, I_z$) were not used. In 66 electrodes there is one "Ground" and one "Reference". So, we call the helmet a 64-channel helmet.

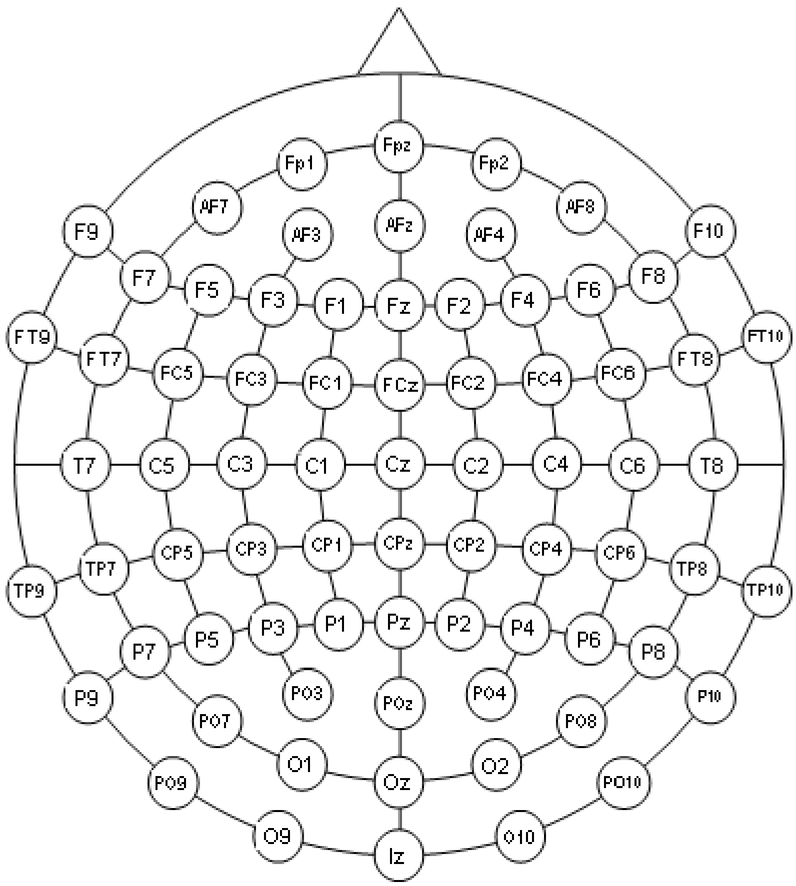

Figure 5.8. The layout of an EasyCap-M1 74-electrode helmet. Only 66 electrodes were used in our experiments, and the other 8 electrodes ($F_{pz}, F_9, F_{10}, P_9, P_{10}, O_9, O_{10}, I_z$) were not used. In 66 electrodes there is one "Ground" and one "Reference". So, only 64-channel data were used for solving inverse problems.

The subject puts the right hand in the warm water (40°C) for 1 minute, then rests in the air for 5 minutes. Then, put right hand in the cold water (4°C) for 1 minute, then rest in the air for 5 minutes. Then put the left hand in the warm water (40°C) for 1 minute, then rest in the air for 5 minutes. Then, put left hand in the cold water (4°C) for 1 minute, then rest in the air for 5 minutes. This is one trial of experiment. The experimenter repeats 3 trials of experiment.

We used FieldTrip [34], MNE [35], and FreeSurfer [36] to create a template head model and a template source model (see Fig. 5.9). Head model contains the geometrical and electrical/magnetic properties of the head, while source model provides the locations of all possible sources.

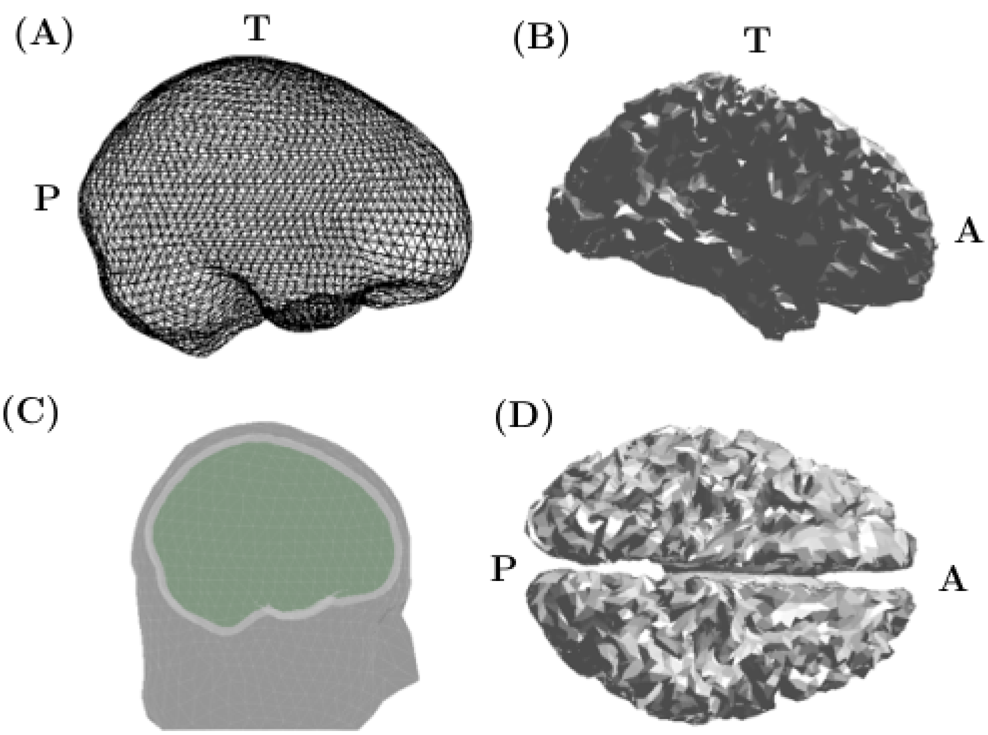

Figure 5.9. Head Model and Source Model. **(A)** Head model contains the geometrical and electrical/magnetic properties of the head. **(B)** Source model (lateral view) provides the locations of all possible sources. **(C)** The alignment of head model and source model. **(D)** Source model (top view). T: top, A: anterior, P: posterior.

We applied the harmonic function method to the real data of pain study, and find that there are strong activities near prefrontal cortex and anterior cingulate cortex (see Fig. 5.10 and Fig. 5.11), of which both are reported to be related to the pain processing in the brain [37].

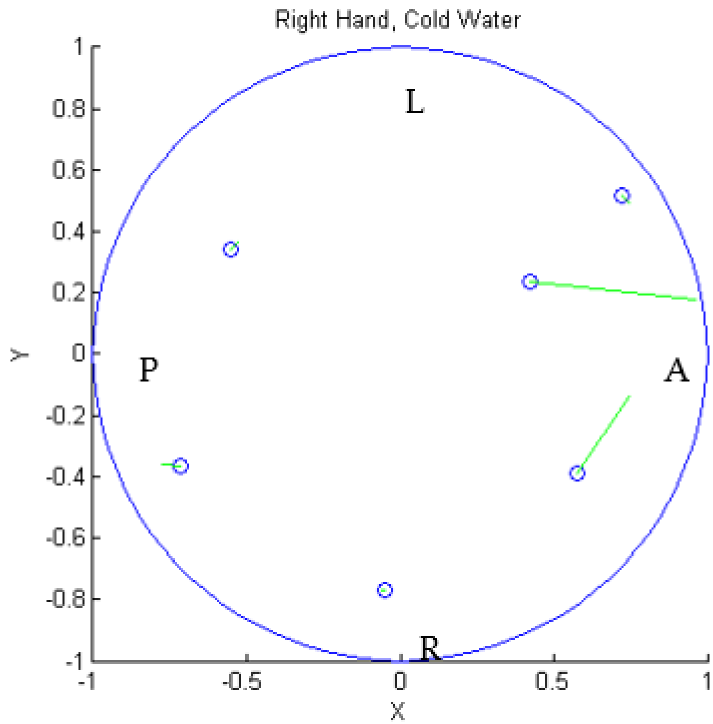

Figure 5.10. Source reconstruction from one averaged measurement on the scalp. Because the sampling frequency is 1000 Hz, the averaged measurement at one instant is the average of the following 1000 measurements. It shows that there are strong activities near prefrontal cortex and anterior cingulate cortex.

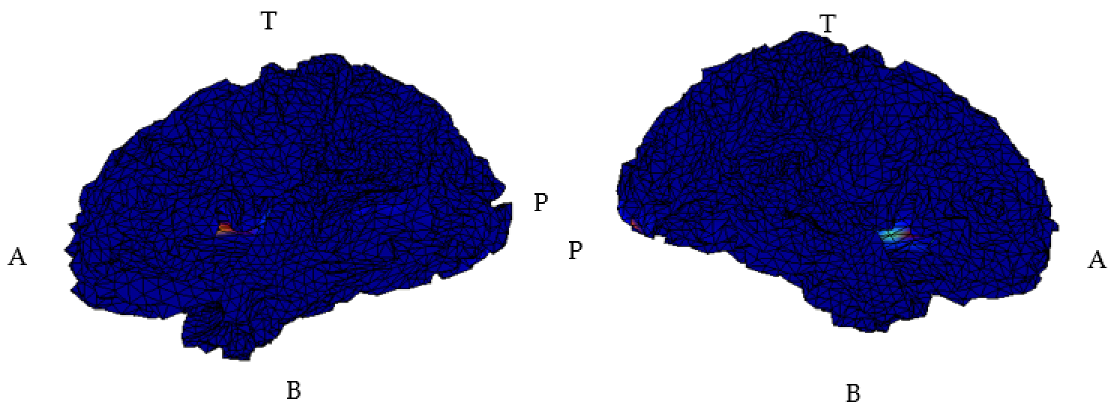

Figure 5.11. Source reconstruction from one averaged measurement on the scalp. Because the sampling frequency is 1000 Hz, the averaged measurement at one instant is the average of the following 1000 measurements. It shows that there are strong activities near prefrontal cortex and anterior cingulate cortex. Also, the response in the left brain is stronger than the response in the right brain, which is consistent with the expectation because the pain stimulus is applied to the right hand. T: top, B: bottom, A: anterior, P: posterior.

CHAPTER 6

Conclusions and Future Work

In this dissertation we studied a harmonic function method for dipolar source reconstruction, and applied the method to the real pain data. Our result showed that when the hand is in the cold water there are strong activities near the prefrontal cortex and the anterior cingulate cortex, which is consistent with the published result [37]. We also provided a better error estimate than Chafik *et al.* because evidence showed that Chafik's estimate may be wrong in some cases.

In chapter 2 we reviewed some preliminaries, such as the fundamental solutions of the Laplacian equation and Sobolev space. In chapter 3 we studied the theory of inverse source problem, especially a harmonic function method for the dipolar source reconstruction. In chapter 4 we derived error estimate for the harmonic function method and compared our result with Chafik's estimate. It is shown by numerical examples that the estimate provided by Chafik *et al.* may be wrong in some cases. Finally, in chapter 5 we did data simulation and applied the harmonic function method to the real pain data, and got good results of dipole source reconstruction, showing that the prefrontal cortex and the anterior cingulate cortex may be the areas related to the pain processing in the brain.

In the future, we plan to extend the harmonic function method to 3D case and applied this method to other realistic areas. Since the estimation of the number of dipoles relies on the calculation of the rank of the measurement matrix, which is significantly affected by the noise, we hope to find some way to solve or circumvent this problem.

We may also compare the efficiency and efficacy of the harmonic function method with other existing reconstruction methods, such as minimum norm estimates (MNE) [38], low resolution electrical tomography (LORETA) [39, 40] or multiple-signal classification algorithm (MUSIC) [41, 42], etc.

APPENDIX A

Some Important Algorithms

A.1 Romberg Integration

Romberg integration [43] is a recursive method for numerically calculating the definite integral

$$I = \int_a^b f(x)dx.$$

A.1.1 Romberg Algorithm

Let $R(n,0)$ be the trapezoid estimate with 2^n subintervals. Then, we get the recursive form of Romberg integration.

$$\begin{cases} R(0,0) = \frac{1}{2}(b-a)[f(a)+f(b)] \\ R(n,0) = \frac{1}{2}R(n-1,0) + h_n \sum_{i=1}^{2^{n-1}} f(a+(2i-1)h_n) \end{cases},$$

and

$$R(n,m) = R(n,m-1) + \frac{1}{4^m-1}[R(n,m-1) - R(n-1,m-1)],$$

where $0 \leq n \leq M$ and $0 \leq m \leq n$. In practice, $M = 10$ is usually enough to get an accurate integral. Also, as M increase the computational load increases exponentially.

The pseudocode for Romberg algorithm is as follows.

Algorithm 1 Romberg Algorithm

procedure ROMBERG

  input a, b, M

  $h \leftarrow b - a$

  $R(0,0) \leftarrow \frac{1}{2}(b-a)[f(a) + f(b)]$

  for $n = 1 : M$ **do**

    $h \leftarrow h/2$

    $R(n,0) \leftarrow \frac{1}{2}R(n-1,0) + h\sum_{i=1}^{2^{n-1}} f(a + (2i-1)h)$

    for $m = 1 : n$ **do**

      $R(n,m) \leftarrow R(n,m-1) + \dfrac{R(n,m-1) - R(n-1,m-1)}{4^m - 1}$

  output $R(n,m) \quad (0 \le n \le M, 0 \le m \le n)$

APPENDIX B

Some Important Theorems

B.1 Divergence Theorem

The divergence theorem has a significant importance in the study of partial differential equations [44].

Let Ω be a bounded domain in R^3 satisfying the following conditions:

1. The boundary $\Gamma := \partial\Omega$ has a finite number of smooth surfaces. A smooth surface is a level surface of a C^2 function with nonvanishing gradient.
2. Any straight line parallel to any of the coordinate axes either intersects Γ at a finite number of points or has a whole interval common with Γ.

Let $\mathbf{n} = (n_x, n_y, n_z)$ be the unit outer normal vector to Γ. Let $\mathbf{V}(x, y, z) = (P(x, y, z), Q(x, y, z), R(x, y, z))$ be a vector field defined in the closure $\overline{\Omega}$ of Ω such that its component functions P, Q, R are in $C^1(\Omega)$ and in $C^0(\overline{\Omega})$.

If $\iiint_\Omega \left(\frac{\partial P}{\partial x} + \frac{\partial Q}{\partial y} + \frac{\partial R}{\partial z}\right) dxdydz$ is convergent, then

$$\iiint_\Omega \left(\frac{\partial P}{\partial x} + \frac{\partial Q}{\partial y} + \frac{\partial R}{\partial z}\right) dxdydz = \iint_\Gamma (Pn_x + Qn_y + Rn_z)ds,$$

or in compact notation,

$$\int_\Omega \operatorname{div} \mathbf{V} dv = \int_\Omega \nabla \cdot \mathbf{V} dv = \int_\Gamma \mathbf{V} \cdot \mathbf{n} ds.$$

B.2 Green's Identities

We get two Green's identities using the divergence theorem.

If $u \in C^2(\mathbb{R}^3)$, then the gradient of u is

$$\nabla u = \operatorname{grad} u = \left(\frac{\partial u}{\partial x}, \frac{\partial u}{\partial y}, \frac{\partial u}{\partial z}\right),$$

and the Laplacian of u is

$$\Delta u = \nabla^2 u = \nabla \cdot \nabla u = \text{div grad}\, u = \frac{\partial^2 u}{\partial x^2} + \frac{\partial^2 u}{\partial y^2} + \frac{\partial^2 u}{\partial z^2}.$$

It is easy to verify the differential identity

$$u\nabla^2 w = \nabla \cdot (u\nabla w) - (\nabla u) \cdot (\nabla w).$$

$$\begin{aligned}
& \nabla \cdot (u\nabla w) - (\nabla u) \cdot (\nabla w) \\
= & \begin{bmatrix} \dfrac{\partial}{\partial x} \\ \dfrac{\partial}{\partial y} \\ \dfrac{\partial}{\partial z} \end{bmatrix} \cdot \begin{bmatrix} uw_x \\ uw_y \\ uw_z \end{bmatrix} - \begin{bmatrix} u_x \\ u_y \\ u_z \end{bmatrix} \cdot \begin{bmatrix} w_x \\ w_y \\ w_z \end{bmatrix} \\
= & \left(\frac{\partial (uw_x)}{\partial x} + \frac{\partial (uw_x)}{\partial y} + \frac{\partial (uw_x)}{\partial z} \right) - (u_x w_x + u_y w_y + u_z w_z) \\
= & (u_x w_x + uw_{xx} + u_y w_y + uw_{yy} + u_z w_z + uw_{zz}) - (u_x w_x + u_y w_y + u_z w_z) \\
= & uw_{xx} + uw_{yy} + uw_{zz} \\
= & u\nabla^2 w.
\end{aligned}$$

REFERENCES

[1] N.K. Logothetis. What we can do and what we cannot do with fMRI. *Nature*, 453(7197):869–878, 2008.

[2] B. He and J. Lian. High-resolution spatio-temporal functional neuroimaging of brain activity. *Crit Rev Biomed Eng*, 30:283–306, 2002.

[3] P.L. Nunez. *Electric Fields of the Brain: The Neurophysics of EEG.* Oxford University Press, 1981.

[4] R. Grave de Peralta Menendez, S.L. Gonzalez Andino, S. Morand, C.M. Michel, and T. Landis. Imaging the electrical activity of the brain: ELECTRA. *Human Brain Mapping*, 9(1):1–12, 2000.

[5] C.M. Michel, M.M. Murray, G. Lantz, S. Gonzalez, L. Spinelli, and R. Grave de Peralta. EEG source imaging. *Clinical Neurophysiology*, 115(10):2195–2222, 2004.

[6] R. Grech, T. Cassar, J. Muscat, K.P. Camilleri, S.G. Fabri, M. Zervakis, P. Xanthopoulos, V. Sakkalis, and B. Vanrumste. Review on solving the inverse problem in EEG source analysis. *Journal of NeuroEngineering and Rehabilitation*, 5(1):25, 2008.

[7] V. Isakov. *Inverse Problems for Partial Differential Equations.* Springer, 2nd edition, 2005.

[8] S. Vessella. Locations and strengths of point sources: stability estimates. *Inverse Problems*, 8(6):911, 1992.

[9] A. El Badia and T. Ha-Duong. An inverse source problem in potential analysis. *Inverse Problems*, 16(3):651–663, 2000.

[10] M. Chafik, A. El Badia, and T. Ha-Duong. On some inverse eeg problems. *Inverse Problems in Engineering Mechanics II*, pages 537–544, 2000.

[11] T. Nara and S. Ando. A projective method for an inverse source problem of the poisson equation. *Inverse Problems*, 19(2):355–369, 2003.

[12] H. Kang and H. Lee. Identification of simple poles via boundary measurements and an application of eit. *Inverse Problems*, 20(6):1853, 2004.

[13] A. El Badia. Inverse source problem in an anisotropic medium by boundary measurements. *Inverse Problems*, 21(5):1487, 2005.

[14] L. Baratchart, A. Ben Abda, F. Ben Hassen, and J. Leblond. Recovery of pointwise sources or small inclusions in 2d domains and rational approximation. *Inverse Problems*, 21(1):51, 2005.

[15] Y.S. Chung and S.Y. Chung. Identification of the combination of monopolar and dipolar sources for elliptic equations. *Inverse Problems*, 25(8):085006, 2009.

[16] D. Kandaswamy, T. Blu, and D. van de Ville. Analytic sensing: Noniterative retrieval of point sources from boundary measurements. *SIAM Journal on Scientific Computing*, 31(4):3179–3194, 2009.

[17] T. Nara and S. Ando. Direct localization of poles of a meromorphic function from measurements on an incomplete boundary. *Inverse Problems*, 26(1):015011, 2010.

[18] A. El Badia and T. Nara. An inverse source problem for helmholtz's equation from the cauchy data with a single wave number. *Inverse Problems*, 27(10):105001, 2011.

[19] M. Clerc, J. Leblond, J.-P. Marmorat, and T. Papadopoulo. Source localization using rational approximation on plane sections. *Inverse Problems*, 28(5):055018, 2012.

[20] R. Mdimagh and I. Ben Saad. Stability estimates for point sources identification problem using reciprocity gap concept via the helmholtz equation. *Applied Mathematical Modelling*, 40(17-18):7844–7861, 2016.

[21] L.C. Evans. *Partial Differential Equations: Second Edition (Graduate Studies in Mathematics)*. American Mathematical Society, 2010.

[22] A. Friedman. *Foundations of Modern Analysis (Dover Books on Mathematics)*. Dover Publications, 2010.

[23] F. Treves. *Basic Linear Partial Differential Equations*. DOVER PUBN INC, 2006.

[24] S. Andrieux, A. Ben Abda, and H.D. Bui. Reciprocity principle and crack identification. *Inverse Problems*, 15(1):59, 1999.

[25] G. Alessandrini. Stable determination of conductivity by boundary measurements. *Applicable Analysis*, 27(1-3):153–172, 1988.

[26] G. Alessandrini and E. DiBenedetto. Determining 2-dimensional cracks in 3-dimensional bodies- uniqueness and stability. *Indiana University Mathematics Journal*, 46(1):1–82, 1997.

[27] A. El Badia and A. El Hajj. Hölder stability estimates for some inverse pointwise source problems. *Comptes Rendus Mathematique*, 350(23-24):1031–1035, 2012.

[28] A. El Badia and A. El Hajj. Stability estimates for an inverse source problem of helmholtzs equation from single cauchy data at a fixed frequency. *Inverse Problems*, 29(12):125008, 2013.

[29] B. Abdelaziz, A. El Badia, and A. El Hajj. Direct algorithm for multipolar sources reconstruction. *Journal of Mathematical Analysis and Applications*, 428(1):306–336, 2015.

[30] B. Abdelaziz, A. El Badia, and A. El Hajj. Direct algorithms for solving some inverse source problems in 2d elliptic equations. *Inverse Problems*, 31(10):105002, 2015.

[31] A. El Badia, A. El Hajj, M. Jazar, and H. Moustafa. Lipschitz stability estimates for an inverse source problem in an elliptic equation from interior measurements. *Applicable Analysis*, 95(9):1873–1890, 2015.

[32] A. El Badia and T. Nara. Inverse dipole source problem for time-harmonic maxwell equations: algebraic algorithm and hlder stability. *Inverse Problems*, 29(1):015007, 2013.

[33] Easycap-m1 74-electrode layout. `http://www.easycap.de/easycap/e/electrodes/10_M01.htm`, 2016.

[34] R. Oostenveld, P. Fries, E. Maris, and J.-M. Schoffelen. FieldTrip: Open source software for advanced analysis of MEG, EEG, and invasive electrophysiological data. *Computational Intelligence and Neuroscience*, 2011:1–9, 2011.

[35] A. Gramfort, M. Luessi, E. Larson, D.A. Engemann, D. Strohmeier, C. Brodbeck, L. Parkkonen, and M.S. Hmlinen. MNE software for processing MEG and EEG data. *NeuroImage*, 86:446–460, 2014.

[36] A.M. Dale, B. Fischl, and M.I. Sereno. Cortical surface-based analysis. *NeuroImage*, 9(2):179–194, 1999.

[37] P.N. Fuchs, Y.B. Peng, J.A. Boyette-Davis, and M.L. Uhelski. The anterior cingulate cortex and pain processing. *Frontiers in Integrative Neuroscience*, 8, 2014.

[38] M.S. Hämäläinen and R.J. Ilmoniemi. Interpreting magnetic fields of the brain: minimum norm estimates. *Medical & Biological Engineering & Computing*, 32(1):35–42, 1994.

[39] R.D. Pascual-Marqui. Review of methods for solving the eeg inverse problem. *International Journal of. Bioelectromagnetism*, 1(1):75–86, 1999.

[40] S. Baillet. Toward functional brain imaging of cortical electrophysiology markovian models for magneto and electroencephalogram source estimation and experimental assessments. *Orsay, France*, 1998.

[41] S. Baillet, J.C. Mosher, and R.M. Leahy. Electromagnetic brain mapping. *IEEE Signal Processing Magazine*, 18(6):14–30, 2001.

[42] J.C. Mosher, P.S. Lewis, and R.M. Leahy. Multiple dipole modeling and localization from spatio-temporal MEG data. *IEEE Transactions on Biomedical Engineering*, 39(6):541–557, 1992.

[43] D.R. Kincaid and E.W. Cheney. *Numerical Analysis: Mathematics of Scientific Computing*. Brooks Cole, 3rd edition, 2001.

[44] E.C. Zachmanoglou and D.W. Thoe. *Introduction to Partial Differential Equations with Applications*. The Williams & Wilkins Company, 1976.

BIOGRAPHICAL STATEMENT

The author Hongguang Xi was born in China. He received a Bachelor's Degree from China Agricultural University in the area of Applied Physics in 1996. He received a Master's degree from Tongji University in the area of Biomedical Engineering in 2007, and a Master's degree from the University of Texas at Arlington in the area of Applied Mathematics in 2012. His research interests include computational neuroscience, dynamical systems, numerical analysis, and data analysis. During the Ph.D. study and this dissertation, he worked extensively on the the theory and application of the source reconstruction in the EEG pain data. After graduating with his Ph.D., he would like to pursue a position to which his expertise in analysis and computation could contribute. He received Mathematics Academic Excellence Scholarship in 2014. He is a member of American Mathematics Society (AMS) and Society of Industrial and Applied Mathematics (SIAM) since 2010.